HDL-TR-1939

December 1980

AD-A094 843

Aerosol Discrimination by Electronic High- and Low-Pass Filtering

by Dennis W. McGuire
Michael Conner
Theodore H. Hopp

U.S. Army Electronics Research
and Development Command
Harry Diamond Laboratories
Adelphi, MD 20783

Approved for public release; distribution unlimited.

REPORT DOCUMENTATION PAGE

READ INSTRUCTIONS BEFORE COMPLETING FORM

1. REPORT NUMBER: HDL-TR-1939	2. GOVT ACCESSION NO.
3. RECIPIENT'S CATALOG NUMBER	
4. TITLE (and Subtitle): Aerosol Discrimination by Electronic High- and Low-Pass Filtering	5. TYPE OF REPORT & PERIOD COVERED: Technical Report
	6. PERFORMING ORG. REPORT NUMBER
7. AUTHOR(s): Dennis W. McGuire Michael Conner Theodore H. Hopp	8. CONTRACT OR GRANT NUMBER(s)
9. PERFORMING ORGANIZATION NAME AND ADDRESS: Harry Diamond Laboratories 2800 Powder Mill Road Adelphi, MD 20783	10. PROGRAM ELEMENT, PROJECT, TASK AREA & WORK UNIT NUMBERS: Program Ele: 62603A DA: 1L162603AH18
11. CONTROLLING OFFICE NAME AND ADDRESS: U.S. Army Armament Research and Development Command Dover, NJ 07801	12. REPORT DATE: December 1980
	13. NUMBER OF PAGES: 77
14. MONITORING AGENCY NAME & ADDRESS(if different from Controlling Office)	15. SECURITY CLASS. (of this report): UNCLASSIFIED
	15a. DECLASSIFICATION/DOWNGRADING SCHEDULE

16. DISTRIBUTION STATEMENT (of this Report)

Approved for public release; distribution unlimited.

17. DISTRIBUTION STATEMENT (of the abstract entered in Block 20, if different from Report)

18. SUPPLEMENTARY NOTES

DRCMS Code: 36KA600062603
HDL Project: A18032

19. KEY WORDS (Continue on reverse side if necessary and identify by block number)

Aerosol discrimination
Optical fuzes
Signal processing
Aerosol scattering
Active optical sensors
Target discrimination
optical detectors
Prox fuzes

20. ABSTRACT (Continue on reverse side if necessary and identify by block number)

Two electronic techniques are investigated for discriminating between aerosol and rigid-target (such as aircraft and terrain) return signals in pulsed active optical sensors (proximity fuzes). Short transmitter pulses approximately 5 to 10 ns full width at half maximum are considered in systems with pencil-beam influence patterns. Relative pulse stretching of aerosol returns is exploited for discrimination by using either a differentiating

20. ABSTRACT (Cont'd)

circuit or a low-pass filter to bring out pulse-speed or pulse-width differences. The investigations involve modeling and analysis, as well as testing the discrimination schemes with measured aerosol-return signals from cumulus clouds. Both techniques are found to be potentially effective for designing proximity fuzes that reject aerosol signals.

CONTENTS

FIGURES

FIGURES (Cont'd)

TABLES

1. INTRODUCTION

Two methods for distinguishing between aerosol- and legitimate target-return signals in pulsed, pencil-beam active optical fuze (AOF) systems have been investigated. The methods are based on the fact that aerosol-return pulses are distorted relative to legitimate returns; aerosol returns are generally more stretched out in time than legitimate target returns. One of the methods, which involves the approximate mathematical differentiation of the return signal by electronic means, has been rather thoroughly investigated and is emphasized in this report. The other, basically a signal integration or low-pass filter scheme, has had only a preliminary investigation, but will be pursued further because superior noise performance is expected with it.

The use of a relatively fast differentiation circuit in the receiver has been investigated on the basis of modeled cloud returns and also of cloud backscatter data. In the latter case, cloud-return pulses recorded during helicopter flight tests were used as test signals. Thus far, the data used have been limited to a small number of test pulses (10) and to returns obtained with an 11-ns full-width-at-half-maximum (FWHM) GaAs laser pulse. Now that data are available for GaAs laser pulses as short as 5 ns and are in a form permitting automatic processing and analysis, it will be possible to test discrimination schemes with a great deal of measured data. The importance of pulse width for discrimination is that shorter pulses are distorted more than longer ones, so that discrimination can be more effectively accomplished with shorter pulses.

The low-pass filter scheme investigated involves normalizing each received pulse and passing it through a low-pass filter. This process tends to make cloud returns larger relative to legitimate target returns; the process thus provides a basis on which discrimination can be made, without degrading the input signal-to-noise ratio (SNR). In fact, an improved SNR is expected. This technique was tested for various filter cutoffs using the same data sample employed to test the differentiation scheme. This method has not yet been analyzed with modeled cloud returns.

This report discusses and summarizes the results of the foregoing investigations. Section 2 is concerned with the differentiation method as applied to modeled cloud-return pulses. Questions of implementability, SNR degradation, and the validity of the modeled cloud-return pulses are considered. Section 3 summarizes the results of applying the differentiation scheme to measured cloud-return pulses, and section 4 does the same for the low-pass filter method. Finally, section 5 is an overall discussion indicating the current lines of the research on the discrimination problem.

2. AEROSOL DISCRIMINATION BY DIFFERENTIATION

A pulsed, pencil-beam AOF operating at some convenient repetition rate is assumed; individual pulses are assumed to have an FWHM in the neighborhood of 5 ns. The receiver system is assumed to have a photodetector-amplifier combination that can detect 5-ns return pulses with reasonable fidelity. The discriminator is a simple differentiation circuit connected to the output of the receiver amplifier, as shown in figure 1. The output signal e(t) from the differentiator will have a positive and then a negative-going peak. One or both of these peaks will be detected by subsequent circuitry, and a decision reached by comparison of the peaks to a preselected threshold; figure 2 illustrates this idea. Note that the resistance R may be the input resistance of an amplification stage.

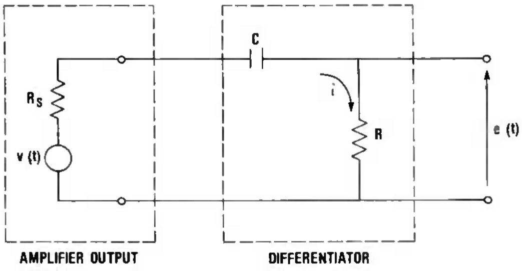

Figure 1. Schematic of discriminator.

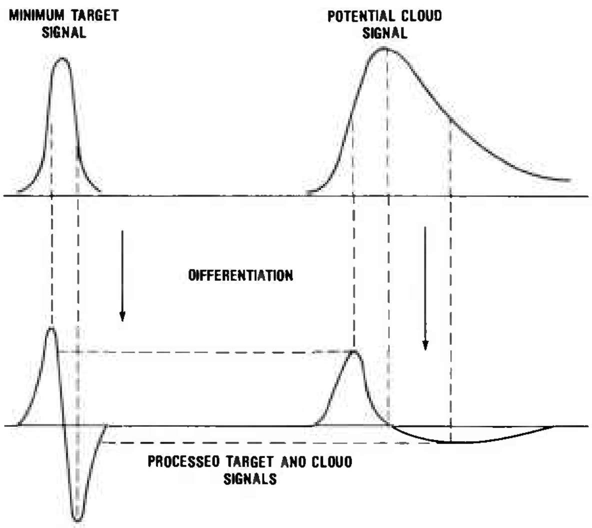

Figure 2. Illustration of idea of derivative discrimination.

Typical values of the amplifier output resistance, R_S, can be expected to lie in the 30 to 50 ohm range. Although it is true that R_S and R will have some stray capacitance associated with them, and that similar parasitic capacitance can arise from active circuits in parallel with these resistances, we think that, by careful design, it would be possible to implement the differentiator of figure 1, for R in the 30 to 50 ohm range, with an effective C of 1 to 2 pF. What kind of performance would such a differentiator have for 5-ns pulses? Answering this question requires the analysis of the circuit of figure 1.

2.1 Circuit Analysis of Differentiator

The basic differential equation governing the circuit dynamics is

$$\frac{di}{dt} + \frac{i}{\tau} = \frac{1}{R_T}\frac{dv}{dt} \quad , \qquad (1)$$

where i is amplifier output current, $\tau = R_T C$, $R_T = R_S + R$, and v is the amplifier source voltage. The general solution of equation (1) can be written as

$$i(t) = a \exp(-t/\tau) + i_p(t) \quad , \qquad (2)$$

where $i_p(t)$ is a particular solution and a is an arbitrary constant. A particular solution can be obtained in terms of a Fourier analysis of v(t). Let

$$v(t) = \int_{-\infty}^{+\infty} A(\omega) \sin\left[\omega t + \alpha(\omega)\right] d\omega \quad . \qquad (3)$$

Then it can be shown that a particular solution of (1) is

$$i_p(t) = \frac{1}{R_T}\int_{-\infty}^{+\infty} \frac{A(\omega)}{\sqrt{1 + \frac{1}{\omega^2\tau^2}}} \sin\left[\omega t + \alpha(\omega) + \tan^{-1}\left(\frac{1}{\omega\tau}\right)\right] d\omega \quad . \qquad (4)$$

The combination of equations (2) and (4) is not particularly convenient for determining the performance of the circuit as a differentiator. It is however possible to express the i_p of equation (4) in a form more suitable for our purposes.

It can be shown (see app A) that

$$R_T i_p(t) = \tau \frac{dv}{dt} - \tau^2 \frac{d^2v}{dt^2} + \tau^3 \frac{d^3v}{dt^3} - \tau^4 \frac{d^4v}{dt^4} + \cdots \quad , \tag{5}$$

which provides a computational basis for determining how close to an actual differentiator the circuit in question is, depending on the circuit time constant τ and the input pulse $v(t)$.

The infinite series of equation (5) can be summed in a particularly convenient form when

$$v(t) = V_0 \cos^2 \frac{\pi t}{2T} \tag{6}$$

for $-T \le t \le T$, and vanishes otherwise. One finds in this case (see app A) that

$$R_T i_p(t) = \tau \frac{dv}{dt}\left(\frac{1}{1 + q^2}\right) - \tau^2 \frac{d^2v}{dt^2}\left(\frac{1}{1 + q^2}\right) \quad , \tag{7}$$

where

$$q = \frac{\pi\tau}{T} \quad . \tag{8}$$

A plot showing the comparative size of the terms on the right-hand side of equation (7) is given in figure 3 for $R = R_S = 50$ ohms, $C = 1$ pF, and $T = 5$ ns (T is the FWHM of $v(t)$ as given by equation (6)). As can be seen, for these parameters our circuit is indeed a good differentiator. An analysis of the effect of the transient term in the solution (see eq (2)) shows that the effect is negligible.

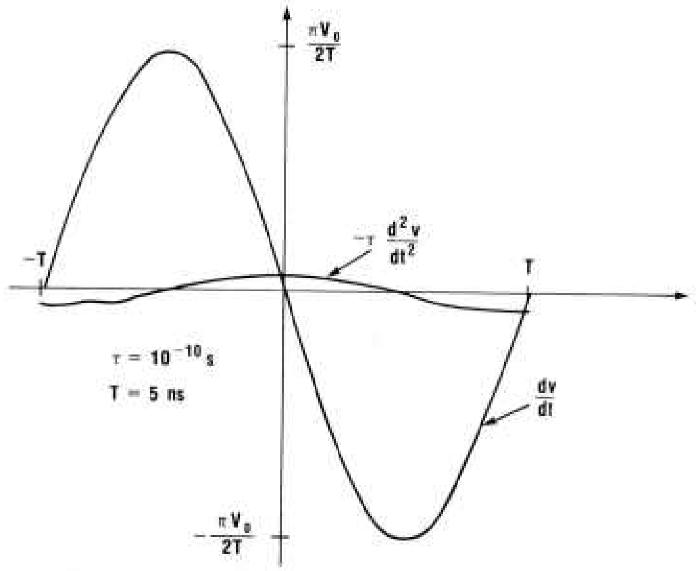

Figure 3. Comparative size of two terms on right of equation (7) for $R = R_S = 50$ ohms, $C = 1$ pF, and $T = 5$ ns.

2.2 Aerosol-Return Pulses

An AOF in the presence of aerosol will receive backscattered signals which might be mistaken for legitimate target signals. In this section, a general and effective method for calculating such return signals is outlined. This method has been computerized for a certain class of aerosol distributions and used to calculate aerosol-return signals, which have in turn been used to test the discriminator being discussed.

Let $P(t)$ and $V(t)$ denote the instantaneous transmitted power and aerosol-return signal, respectively, and let x denote range from the transceiver measured along its pencil-beam influence pattern. Define the function of range $C(x)$ by

$$C(x) = \mu(x) \exp\left[-2 \int_0^x \sigma(s)\, ds\right] , \tag{9}$$

where $\mu(x)$ and $\sigma(x)$ are, respectively, the volume backscatter and extinction coefficients of the aerosol at range x. Finally, let R(x) denote the range sensitivity function of the AOF. Then V(t) can be expressed as

$$V(t) = K \int_0^{\infty} P(t - \tau)\, C\left(\frac{c\tau}{2}\right) R\left(\frac{c\tau}{2}\right) d\tau \quad , \tag{10}$$

assuming that signal-distortion effects in the receiver amplifiers are negligible. The factor K is a constant depending on the normalization chosen for R(x) and the units of V(t); c is the speed of light. This result, originally derived by Burroughs,[1] has great generality. It applies to virtually all pencil-beam active optical-detection systems where transmitter and receiver are approximately colocated. Multiple-scattering effects are, however, ignored in deriving equation (10); this is its principal limitation. When aerosol densities are sufficiently high that multiple-scattering effects are appreciable, very sophisticated calculations are needed to determine aerosol-return signals.[2]

A computer program has been written to calculate the integral in equation (10), for various types of P, C, and R; a listing is provided as appendix B. The model chosen for P was the cosine-squared shaped pulse; its pulse width is a variable input parameter in the program. The model chosen for C arises from equation (9) when the extinction and backscatter profiles shown in figure 4 are used. The distance x_0 to the aerosol edge, the length ℓ of the buildup region, as well as the constant values of μ and σ characterizing the aerosol interior, are all input parameters in the program. Two types of range-response characteristics R can be used. One type arises when the transmitter field and receiver field of view are uniform, collimated intersecting pencil beams of very small divergence. The other type corresponds to systems which image both the source laser and its photodetector at a common finite range from the transceiver, where peak response is desired. The program also calculates the derivative of the aerosol-return pulse it determines.

---

[1]H. H. Burroughs, *Computation of Cloud Backscatter Power as a Function of Time for an Active Optical Radar (U)*, Naval Weapons Center, NWC TP 5090 (April 1971). (CONFIDENTIAL)

[2]R. E. Bird, *Calculations of Multiple-Scattering Effects on Active Optical Sensors in Cloud Environments*, Naval Weapons Center, NWC TP 5667 (August 1974).

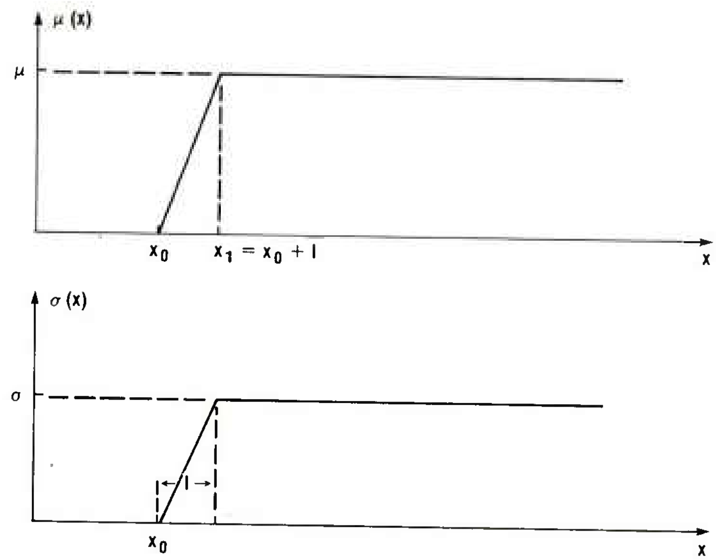

Figure 4. Model profiles of aerosol backscatter and extinction coefficients.

Typical results obtained with the program are shown in figures 5 and 6. Figure 5 shows the calculated aerosol-return pulse in arbitrary units for a 5-ns FWHM transmitter pulse; in this calculation, the AOF is fully immersed in a uniform aerosol having $\sigma = 0.15\ m^{-1}$ and $\mu = 0.008\ m^{-1}str^{-1}$. The range response of the AOF is that due to uniform pencil beams which are fully overlapped from 5.89 m to infinity and partially overlapped from 2.67 to 5.89 m. The σ and μ values used correspond to a rather dense water cloud. Figure 6 shows the derivative of the cloud-return pulse of figure 5. Notice the rather large amount of pulse stretching evident in the cloud-return pulse compared to the transmitter pulse, which has a 5-ns FWHM and a 10-ns width at its base. The return pulse from a legitimate target for this AOF would be expected to be a very close replica of the transmitter pulse. Notice also that the peak value of the derivative of the cloud pulse on its trailing edge is substantially less than that on its leading edge. This asymmetry is caused by the pulse stretching and is a general feature of the calculated results. It suggests that derivative discrimination will be more effective if based on the trailing-edge derivative, at least for symmetrical transmitter pulses.

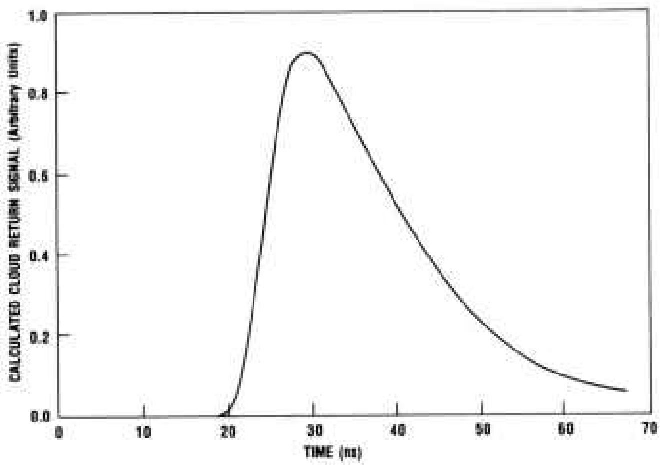

Figure 5. Calculated cloud-return signal in arbitrary units for a 5-ns FWHM cosine-squared transmitter pulse, with system fully immersed in uniform cloud, having $\sigma = 0.15\ m^{-1}$ and $\mu = 0.008\ m^{-1}str^{-1}$.

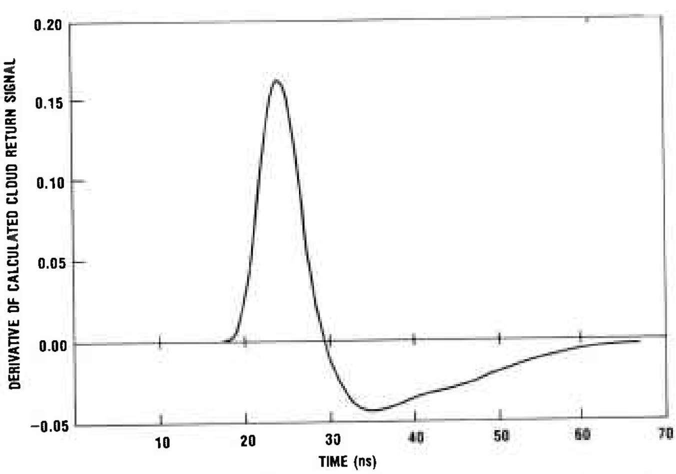

Figure 6. Derivative of calculated cloud-return signal of figure 5.

2.3 Evaluation of Derivative Discrimination without Noise

The basic gauge chosen to evaluate the discrimination scheme is the improvement in target/aerosol contrast produced by the discriminator. Suppose that the AOF without the differentiator receives a signal $V_T(t)$ from some legitimate target in its field of view. This is to be compared with the aerosol signal $V_A(t)$ that the same AOF could receive from some distribution of aerosol. Assuming peak detection, the decision circuitry would be presented with either of two peak signal values, $\hat{V}_T$ and $\hat{V}_A$, and would determine to fire on the basis of how large

the peak signal values happen to be in relation to the predetermined threshold. The function of the discriminator is to reduce $\hat{V}_A$ in relation to $\hat{V}_T$. If the AOF had a differentiation circuit and was peak detecting the differentiated signal, then the decision circuit would be presented with two different peak signal values, say $\hat{V}_T'$ and $\hat{V}_A'$ (assume for specificity that the peak derivative on the trailing edge of the pulse is being detected). A measure of the efficacy of the discriminator is then provided by the ratio

$$F_I = \frac{\hat{V}_T'/\hat{V}_A'}{\hat{V}_T/\hat{V}_A} , \tag{11}$$

which we call the target/aerosol contrast-improvement factor.

It is easy to see that F_I is independent of the amplitudes $\hat{V}_T$ and $\hat{V}_A$ of the return signals $V_T(t)$ and $V_A(t)$. Let

$$V_T(t) = \hat{V}_T U_T(t)$$

and (12)

$$V_A(t) = \hat{V}_A U_A(t) ,$$

where U_T and U_A give the shape of the return signals and are normalized to unit amplitude. Then

$$\dot{V}_T(t) = \hat{V}_T \dot{U}_T(t)$$

and (13)

$$\dot{V}_A(t) = \hat{V}_A \dot{U}_A(t) ,$$

where the dot denotes time differentiation. Let t_0 and t_1 denote the times at which $\dot{V}_T(t)$ and $\dot{V}_A(t)$ achieve their peak values, respectively. Then

$$\hat{V}'_T = \hat{V}_T \dot{U}_T(t_0)$$

and (14)

$$\hat{V}'_A = \hat{V}_A \dot{U}_A(t_1) \quad ,$$

so that

$$F_I = \frac{\dot{U}_T(t_0)}{\dot{U}_A(t_1)} \quad . \tag{15}$$

Equation (15) shows that the same value of F_I is obtained if it is assumed that $V_T(t)$ and $V_A(t)$ both have unit amplitude.

The effect of the discriminator on the SNR is not included in the factor F_I. This effect is considered in section 2.4.

To evaluate the discrimination scheme, a unit-amplitude target pulse $U_T(t)$ having the same width and shape (cosine-squared) as the transmitter pulse is assumed. Then aerosol-return pulse shapes are calculated for various modeled aerosol distributions giving $U_A(t)$. Finally, $\dot{U}_T(t)$ and $\dot{U}_A(t)$ are computed, their peak values noted, and F_I is determined.

Some results of the foregoing evaluation are given in figure 7, where $\dot{U}_A(t_1)$ for the trailing edge of the aerosol return was used. For these results, a uniform density aerosol with an abrupt leading edge was assumed to extend from the in-range cutoff to infinity. The approximate relationship

$$\frac{u}{\sigma} \approx 0.05 \text{ sr}^{-1} \quad , \tag{16}$$

valid for not-too-dense water clouds at the GaAs laser wavelength, was used to eliminate a variable. Two range-response characteristics were

used: the one used for the illustrations of figures 5 and 6, which has a 2.67-m in-range cutoff, and another differing only in that its in-range cutoff is 1.67 m. The figure plots the contrast-improvement factor F_I versus the extinction coefficient, σ, for several cases of transmitter pulse width.

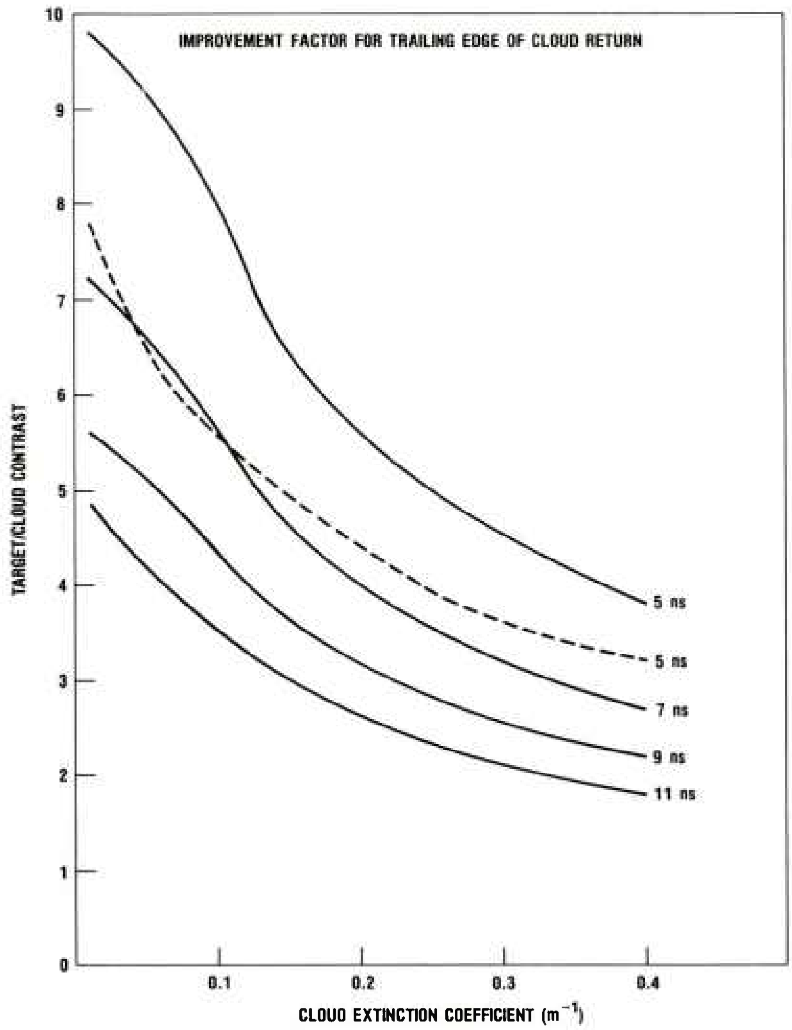

Figure 7. Target/cloud contrast improvement factor versus cloud extinction coefficient for several cases of transmitter pulse width and two range-response characteristics. Solid curves: range law same as in figures 5 and 6, with 2.67-m in-range cutoff. Dotted curve: in-range cutoff is 1.67 m, and beams are fully overlapped from 5.89 m to infinity. FWHM of cosine-squared shaped transmitter pulse is shown next to curves. For all results, uniform-density aerosol with abrupt leading edge assumed to extend from in-range cutoff to infinity.

Extinction coefficients much above the range from 0 to $0.1\ m^{-1}$ are unlikely. For this range of extinction coefficients, figure 7 shows that improvement factors ranging from 3.5 to about 10 can be expected for the systems considered. Improvement decreases with increasing extinction coefficient and transmitter pulse width, as would be expected. The figure also shows that improvement decreases as the in-range hole in the influence pattern gets smaller. This effect is due to the increased length of the aerosol that returns signal from the near ranges, which ranges make the largest contribution to the return signal. The effect could be minimized by reducing the near-range sensitivity of the system to be sufficient for target detection but no greater. Such range-response tailoring is possible through several techniques.

2.4 Noise Degradation

In this section, the effects of noise on the performance of the derivative discriminator are analyzed, subject to certain reasonable assumptions concerning the noise process at the input to the differentiator. The analysis results in a relationship between the mean-square noise voltages at the input and output of the discriminator, and provides an estimate of the output SNR in terms of the input SNR.

Sztankay[3] has discussed the significant noise sources present in direct optical detection systems. Virtually all such sources are of the Johnson or shot noise type, except possibly the avalanche multiplication noise which arises when avalanche photodiodes are used for detection. It therefore seems reasonable to assume that the noise voltage at the output of the receiver amplifier is a stationary Gaussian process with a uniform band-limited power spectral density.

Let $n(t)$ denote the effective noise voltage in series with $v(t)$ and R_S in figure 1, where R_S is assumed noiseless. Since $n(t)$ is assumed to be band-limited white noise, its power spectral density, $S_n(f)$, is given by

$$S_n(f) = A \text{ for } |f| \le B \quad ,$$

and (17)

$$S_n(f) = 0 \text{ for } |f| > B \quad ,$$

[3] *Z. G. Sztankay, Analysis of a Slant-Range Optical Proximity Sensor, Harry Diamond Laboratories, HDL-TR-1625 (July 1973).*

where f is the frequency, A is a positive constant, and B is the noise bandwidth. In equation (17), the noise band has been assumed to have a sharp upper-frequency cutoff (namely B) and no lower-frequency cutoff. It therefore follows that the autocorrelation function, $R_n(\bar{\tau})$, of the noise n is given by

$$R_n(\bar{\tau}) = 2AB \frac{\sin 2\pi B\bar{\tau}}{2\pi B\bar{\tau}} \quad . \tag{18}$$

Since $R_n(0) = \langle n^2 \rangle$, the mean-square noise voltage, it can be seen that

$$A = \frac{\langle n^2 \rangle}{2B} \quad . \tag{19}$$

Now let N(t) denote the noise voltage at the output of the discriminator. By standard results from the theory of random signals and noise,[4] N(t) is a stationary Gaussian process, and its power spectral density $S_N(f)$ is given by

$$S_N(f) = |H|^2 S_n(f) + S_J(f) \quad , \tag{20}$$

where H is the system function of the differentiator (including the source resistance R_S) and $S_J(f)$ is the contribution of the Johnson noise arising in the resistor R. The system function is given in good approximation by

$$H(j\omega) = j\omega R_T C \quad , \quad j = \sqrt{-1} \quad , \tag{21}$$

[4] *Wilbur B. Davenport, Jr., and William L. Root, An Introduction to the Theory of Random Signals and Noise, McGraw-Hill Book Co., Inc., New York (1958).*

where $\omega = 2\pi f$, because the discriminator is very nearly a perfect differentiator for frequencies in the signal band, and consequently for frequencies in the noise band. Since it would be a matter of good engineering practice to arrange that $S_J(f)$ be a negligible part of $S_N(f)$, we ignore it. Thus

$$S_N(f) = \left(\omega R_T C\right)^2 \frac{\langle n^2 \rangle}{2B} \text{ for } |f| \leq B$$

and (22)

$$S_N(f) = 0 \text{ for } |f| > B \quad ;$$

so that the autocorrelation function of $N(t)$ is

$$R_N(\bar{\tau}) = \frac{2\pi^2 R_T^2 C^2 \langle n^2 \rangle}{B} \int_{-B}^{B} f^2 e^{2\pi i f \bar{\tau}} \, df \quad . \tag{23}$$

The main interest lies in $R_N(0) = \langle N^2 \rangle$, the mean-square output noise voltage. By equation (23),

$$\langle N^2 \rangle = \left(2\pi R_T C\right)^2 \langle n^2 \rangle \frac{B^2}{3} \quad , \tag{24}$$

which relates the rms output noise voltage to the input rms noise voltage. Using equation (24), it is not diffcult to obtain a corresponding relation between the input and output SNR. Assuming that $v(t)$ is given by equation (6), the peak values of $e(t)$ are, in very good approximation, $\pm\pi V_0 R_T C/2T$. Thus,

$$(\text{SNR})_{\text{output}} = \frac{\sqrt{3}}{4BT} (\text{SNR})_{\text{input}} \quad , \tag{25}$$

where SNR is taken to mean the ratio of peak signal to rms noise.

For the situation of interest, a reasonable estimate of the coefficient in equation (25) is obtained by putting B = 150 MHz and T = 5 ns. Then $(SNR)_{output} \approx 0.57(SNR)_{input}$, so that the output SNR degrades to something like 60 percent of the input SNR. The SNR reduction occurs because, basically, differentiation is a noise-enhancing process. In a complete evaluation of the discrimination scheme, both F_I and the SNR reduction must be considered; however, the latter effect would be unimportant if a sufficiently high input SNR were obtainable.

2.5 Evaluation of Derivative Discrimination with Noise

The results of sections 2.3 and 2.4 can be combined to provide an overall analysis of derivative discrimination for various realistic situations. In this section, the general outline of such an analysis is discussed and illustrated with concrete examples.

Basic for an evaluation is knowledge of the kinds of aerosol distributions which are likely to be encountered in a given application. This knowledge can take various forms. For a relatively simple analysis, it might be assumed that it is sufficient to consider only uniform aerosol distributions and the maximum signals that they will produce. In this instance, the scope of aerosol conditions could be simply characterized by a range of extinction coefficients or, less simplistically, by a probability distribution of extinction coefficients. A working probability distribution function could be obtained, for example, from an analysis of helicopter flight test data on clouds, obtained by the Harry Diamond Laboratories (HDL). There are, of course, less simple and more realistic ways to proceed. Such procedures would include the effects of bulk aerosol nonuniformities, cloud edge variations, and the encounter geometry.

Another basic element in the evaluation is a specification of the sensing system in terms of generic parameters (such as field of view, range cutoffs, peak output power, and output pulse shape, etc) and a specification of minimum detectable target conditions (minimum target size, maximum target range at which detection is desired, etc). This information, together with some estimation of the significant noise sources in the system, will allow a determination of the minimum target signal that is to be detected and of the probabilities of detection and false alarm with no aerosol present. In addition, using the probability distribution of aerosol extinction levels, the probability distribution of aerosol signals could be determined, and the effect of detection noise then included.

The result of the foregoing would be two probability-distribution curves, one for the detected minimum target signal and one for the detected aerosol signal, assuming for example peak detection. These

curves would be similar to those in figure 8, where the relative location of the peaks of the probability distributions would depend on the specific details in the indicated analysis.

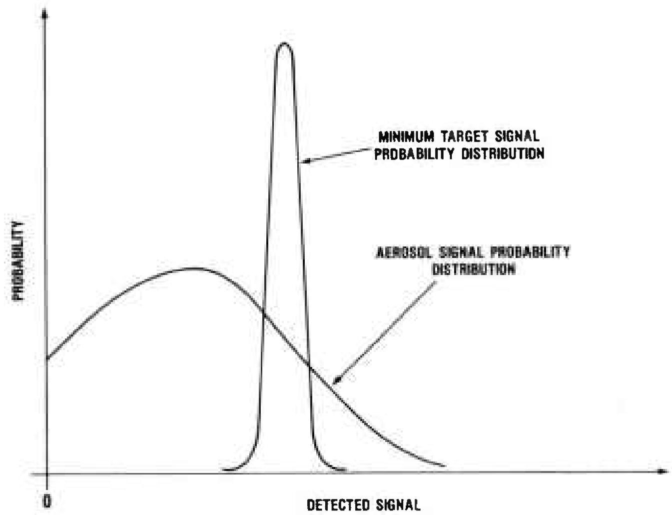

Figure 8. Qualitative appearance of probability distribution curves for detected minimum target and aerosol signals when discriminator is not used.

The effect of introducing the derivative discriminator and, for example, peak detecting the derivative along the trailing edge of the received pulse would be twofold. Both probability distributions would be broadened in accordance with the noise enhancement produced by the discriminator, and the peak of the probability distribution for the detected minimum target signal would be shifted to the right in relation to that for the detected aerosol signal, in accordance with the contrast-improvement factor F_I. The desired final result would be as shown in figure 9, with no overlapping of the tails of the distributions. In general, however, some overlap would occur, and the final step of the analysis would be to determine, for various placements of a threshold level, the probabilities of target detection and false firing on aerosol. In carrying out this last step, additional knowledge about the encounter scenario would be introduced. For example, it may be known that aerosol will be present in only some fractional part of all the possible encounters, or for only some fraction of the time during one mission, so that a scaling down of the aerosol probability distribution is indicated.

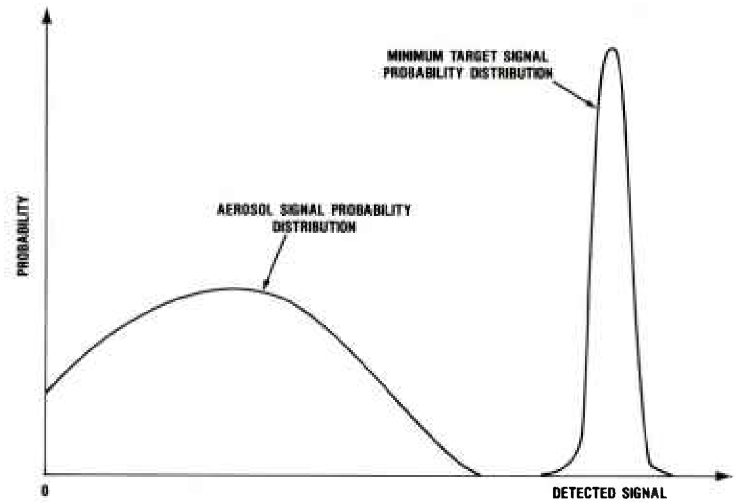

Figure 9. Desired appearance of probability distribution curves for detected minimum target and aerosol signals after discriminator processing.

To make the foregoing outline more concrete, we now analyze a generic example and give numerical results for specific cases. In what follows, the sensing system is assumed to have a transmitter pulse of the form

$$P_0(t) = \bar{P}_0 \cos^2 \frac{\pi t}{2T} \text{ for } -T \leq t \leq T \quad ,$$
$$= 0 \text{ otherwise} \quad , \tag{26}$$

where $P_0(t)$ is the transmitted optical power as a function of time, $\bar{P}_0$ is the peak power, and T is the FWHM of the pulse. The system's range response, R(x), is assumed to arise from uniform pencil beams which are fully overlapped from the range R_F to infinity and partially overlapped between R_0 and R_F ($R_0 < R_F$). The normalization for R(x) is chosen so that $R(x) = x^{-2}$ where the beams are fully overlapped.

If a Lambertian diffuse reflector of diffuse reflectivity ρ_0 intersects the system's pencil-beam influence pattern at range x in the full-overlap region, then the peak received signal power $\hat{P}_T$ will be

$$\hat{P}_T = \bar{P}_0 A \frac{\rho_0 \cos \theta}{\pi x^2} \quad , \tag{27}$$

where A is the area of the receiving aperture and θ is the angle between the reflector normal (at the point of illumination) and the direction of the influence pattern. Minimum detectable target conditions are defined by a minimum reflectivity ρ_0, a maximum range x_{max} at which detection is desired, and a target orientation θ. Taking the latter as $\theta = 0$, the minimum peak received signal power $P_T(min)$ becomes

$$P_T(min) = \bar{P}_0 A \frac{\rho_0}{\pi x_{max}^2} \quad . \tag{28}$$

To obtain the signal levels connected with aerosol backscatter, equations (9) and (10) can be used. Assuming that a uniform aerosol with an abrupt leading edge extended from R_0 to infinity (a condition that gives the highest peak aerosol return signals for given μ and σ), we get

$$P_a(t) = \frac{c}{2} e^{2\sigma R_0} \bar{P}_0 A \int_{\max\left[t-T,\ \frac{2R_0}{c}\right]}^{t+T} \cos^2 \frac{\pi(t-\tau)}{2T} \, e^{-\sigma c \tau} \mu R\left(\frac{c\tau}{2}\right) d\tau \quad , \tag{29}$$

for the instantaneous received aerosol signal power, $P_a(t)$. Let $\hat{P}_a$ denote the maximum value of $P_a(t)$.

Assume that $\mu = 0.05\sigma$ as in equation (16) and let $W(\sigma)$ denote the probability distribution of extinction coefficients: that is, when aerosol is encountered, the probability that its extinction coefficient

lies between σ and $\sigma + d\sigma$ is given by $W(\sigma)\, d\sigma$. The corresponding probability distribution $\rho(\hat{P}_a)$ for $\hat{P}_a$ is then given by

$$\rho\left(\hat{P}_a\right) = W\left[\sigma\left(\hat{P}_a\right)\right] \left|\frac{d\sigma}{d\hat{P}_a}\right| \quad , \tag{30}$$

provided the inverse function $\sigma(\hat{P}_a)$ is uniquely well-defined; equation (29) defines the function $\hat{P}_a(\sigma)$, which must define a one-to-one correspondence between the σ's and the $\hat{P}_a$'s for $\sigma(\hat{P}_a)$ to be uniquely well-defined. This qualification on the validity of equation (30) points out a complication in the analysis which will be avoided here by making a somewhat unrealistic assumption; namely, that $W(\sigma) = 0$ for all $\sigma \geq \sigma_{max}$, where σ_{max} is a fixed maximum extinction coefficient. This is done because, qualitatively, the graph of $\hat{P}_a$ versus σ has the appearance of figure 10, which implies that $\sigma(\hat{P}_a)$ is two-valued for some range of $\hat{P}_a$ values. This feature could be incorporated into equation (30) by using both branches $\sigma_1(\hat{P}_a)$ and $\sigma_2(\hat{P}_a)$ of $\hat{P}_a^{-1}(\sigma)$, namely

$$\rho\left(\hat{P}_a\right) = W\left[\sigma_1\left(\hat{P}_a\right)\right] \left|\frac{d\sigma_1}{d\hat{P}_a}\right| + W\left[\sigma_2\left(\hat{P}_a\right)\right] \left|\frac{d\sigma_2}{d\hat{P}_a}\right| \quad ; \tag{31}$$

however, this would unnecessarily complicate the illustration being developed. Accordingly, σ_{max} is chosen as in figure 10 and the effects of equation (31) are left for a more refined analysis.

Let k denote the overall conversion factor for the receiver that gives the receiver output V for received optical power P through $V = kP$. Then, if the mean-squared noise voltage at the receiver output is $\langle n^2 \rangle$, the probability distribution $p_A(\hat{V}_a)$ of detected peak aerosol signals $\hat{V}_a$ is given by

$$p_A\left(\hat{V}_a\right) = \frac{1}{\sqrt{2\pi \langle n^2 \rangle}} \int_0^{\sigma_{max}} W(\sigma) \exp\left(\frac{-\left[\hat{V}_a - k\hat{P}_a(\sigma)\right]^2}{2\langle n^2 \rangle}\right) d\sigma \quad , \tag{32}$$

where the noise has been assumed Gaussian. The corresponding probability distribution about the minimum target signal $kP_T(\min)$ is

$$p_T\left(\hat{V}_T\right) = \frac{1}{\sqrt{2\pi\langle n^2\rangle}} \exp\left(\frac{-\left[\hat{V}_T - kP_T(\min)\right]^2}{2\langle n^2\rangle}\right) . \qquad (33)$$

Equations (32) and (33) describe the detection situation regarding aerosol signals and the minimum target signal without the use of the derivative discriminator. The same equations continue to describe the situation after processing by the discriminator, provided that the quantities $kP_a(\sigma)$, $kP_T(\min)$, and $\langle n^2\rangle$ are replaced by the appropriate postprocessing values.

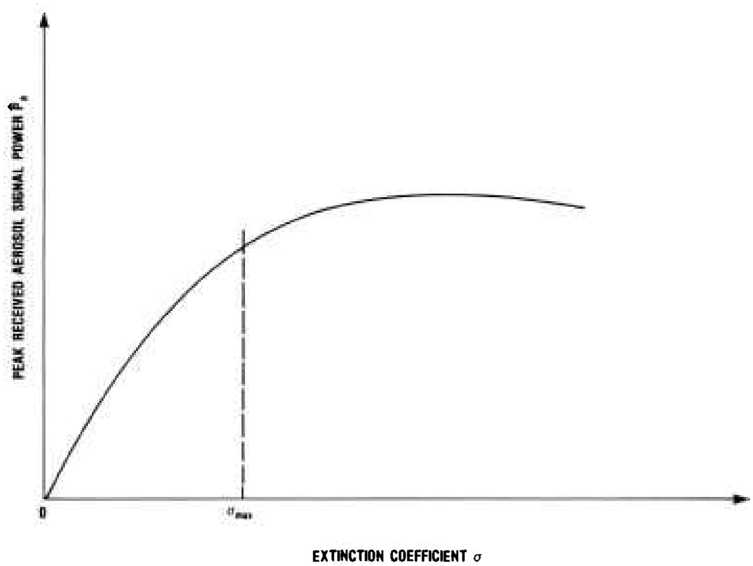

Figure 10. Qualitative variation of peak received aerosol signal power $\hat{P}_a$ with aerosol extinction coefficient σ, showing σ_{max} where probability distribution of extinction coefficients is cut off.

Following section 2.4, since the noise at the discriminator output is Gaussian, the appropriate replacement for $\langle n^2\rangle$ is $\langle N^2\rangle$, which is given by equation (24). Since the peaks of the processed minimum target signal are given in good approximation by $\pm\pi R_T C k P_T(\min)/2T$, the replacement for $kP_T(\min)$ is very nearly $\pi R_T C k P_T(\min)/2T$. Finally, if

peak detection of the derivative along the trailing edge of the return pulse is assumed, the replacement for $k\hat{P}_a(\sigma)$ is (to the approximation just used)

$$k \max \left| R_T C \frac{dP_a(t)}{dt} \right| \quad ,$$

where the maximum is evaluated along the negative-going part of dP_a/dt. Let $\hat{\dot{P}}_a(\sigma)$ denote this maximum for $|dP_a(t)/dt|$, considered as a function of σ.

In order to reach numerical conclusions for specific values of the parameters T, ρ_0, x_{max}, R_F, etc, we must evaluate the integral in equation (32) (and its correspondent for the processed signals) and furthermore be able to integrate over the resulting probability distributions to determine probabilities of detection and false alarm. This can be done without a great deal of numerical integration if two approximations are made, one of which is unfortunately rather crude.

First we approximate $\hat{P}_a(\sigma)$ by a linear variation, that is, $\hat{P}_a(\sigma) \approx m\sigma$, where $m > 0$. That this is reasonable can be seen from figure 11, which plots $\hat{P}_a$ versus σ (computed from eq (29) using the computer program discussed in sect. 2.2) for several values of T, using the range-response parameters $R_0 = 2.67$ m and $R_F = 5.89$ m (the ones used most often in sect. 2.3) and equation (16). Next, we estimate the contrast-improvement factor F_I by its minimum value in the range of σ being considered (fig. 7), thus neglecting its σ-dependence (the T-dependence is, however, retained). Although this approximation is rather crude, it has the convenient effect of estimating $\hat{\dot{P}}_a(\sigma)$ by a linear variation in σ because

$$\hat{P}_a(\sigma) \approx \frac{2T}{\pi} F_I \hat{\dot{P}}_a(\sigma) \quad , \tag{34}$$

as can be readily verified. As a final simplification we assume that the probability distribution of extinction levels σ is

$$\begin{aligned} W(\sigma) &= W_0 \text{ for } 0 \leq \sigma < \sigma_{max} \\ &= 0 \text{ for } \sigma \geq \sigma_{max} \end{aligned} \tag{35}$$

where W_0 is a constant such that $W_0\sigma_{max} = 1$. With these simplifications, the probability distribution p_A of equation (32) can be evaluated in terms of error functions, which in turn have well-known indefinite integrals.

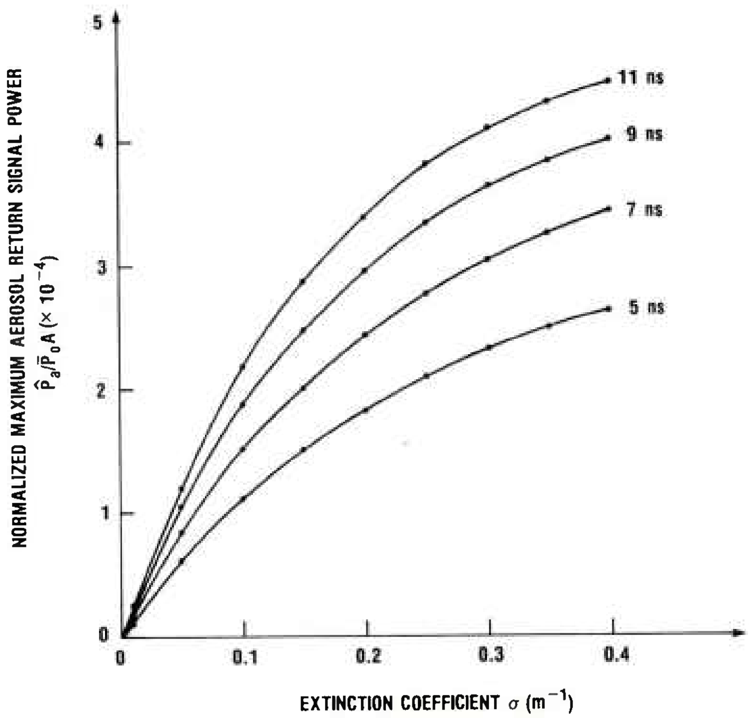

Figure 11. Normalized maximum aerosol-return signal power versus extinction coefficient for several values of the transmitter pulse width. Curves computed from equation (29) using range-response parameters $R_0 = 2.67$ m and $R_F = 5.89$ m. Transmitter pulse-width values are full widths at half maximum.

Define the function p(y) by

$$p(y) = \frac{W_0}{\sqrt{2\pi s^2}} \int_0^{\sigma_{max}} \exp\left[\frac{-1}{2s^2} (y - \lambda\sigma)^2\right] d\sigma \quad , \tag{36}$$

which depends parametrically on s^2 and λ. The probability distribution of equation (32) and its correspondent for the processed aerosol signals are both of the form p(y), and can be obtained explicitly with the parameter identifications given in table 1.

TABLE 1. PARAMETER IDENTIFICATIONS FOR EQUATION (36)

Aerosol signals	s^2	λ
Unprocessed	$\langle n^2 \rangle$	km
Processed	$\langle N^2 \rangle$	$\dfrac{km\pi R_T C}{2TF_I}$

Evaluating the integral in equation (36) one obtains

$$p(y) = \frac{W_0}{2\lambda}\left[\operatorname{erf}\frac{y}{\sqrt{2}s} - \operatorname{erf}\left(\frac{y - \lambda\sigma_{max}}{\sqrt{2}s}\right)\right] \quad . \tag{37}$$

A sketch of the graph of p(y) is given in figure 12, which also shows what p(y) would look like if noise had been ignored. Notice that p(y) has a single maximum at

$$y = y_{max} = \frac{1}{2}\lambda\sigma_{max} \quad , \tag{38}$$

and that the graph is symmetrical about y_{max}.

The probability of false firing on an aerosol signal for a given detection threshold level y_{th} can now be calculated. The desired probability P_F is given by

$$P_F\left(y_{th}\right) = \int_{y_{th}}^{\infty} p(y)\, dy \quad . \tag{39}$$

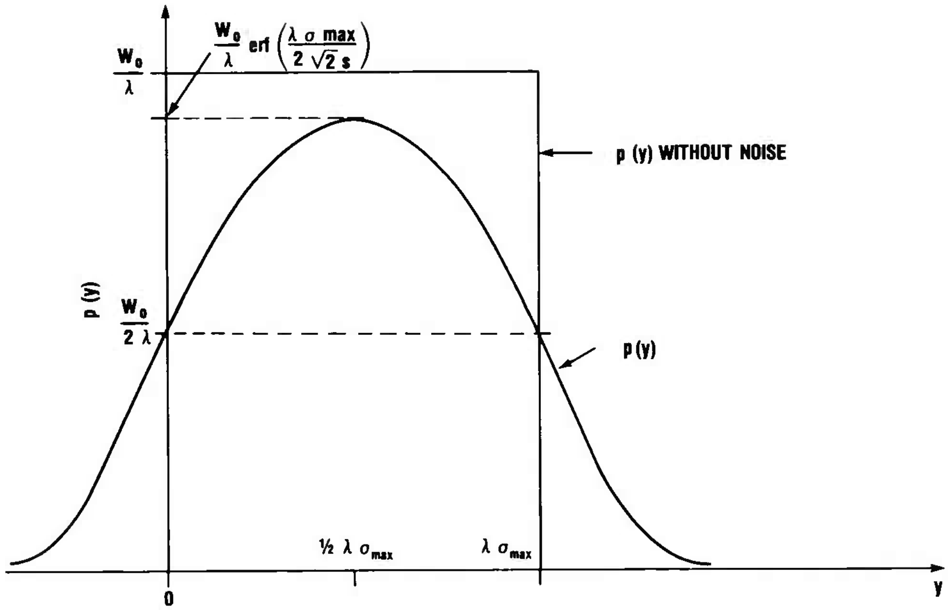

Figure 12. Basic probability distribution of equation (37). Also shown is what p(y) would be without noise.

The integral is readily evaluated, and one finds that

$$\bar{B}P_F(y_{th}) = \frac{1}{\sqrt{\pi}}\left[\exp\left(-x_1^2\right) - \exp\left(-x_2^2\right)\right] - \left(x_2 \text{ erf } x_2 - x_1 \text{ erf } x_1\right) + \frac{2y_{max}}{\sqrt{2s^2}} \quad , \tag{40}$$

where

$$x_1 = \frac{y_{th} - 2y_{max}}{\sqrt{2s^2}} \quad , \tag{41}$$

$$x_2 = \frac{y_{th}}{\sqrt{2s^2}} \quad , \tag{42}$$

$$\bar{B} = \frac{1}{\sqrt{2s^2}} \frac{2\lambda}{W_0} \quad . \tag{43}$$

Since p(y) is normalized so that its integral over all y is unity, P_F gives the probability that when aerosol is encountered a false firing will occur for a single return pulse. To convert P_F into a total mission probability of false alarm on aerosols, one would need to know the average number, N, of transmitted pulses per mission that are returned from aerosols. Then the desired false-alarm probability could be determined as $1 - \left(1 - P_F\right)^N$.

To complete the analysis, we need formulas for the probability of detecting a minimum target signal. Let S denote the signal-to-noise ratio associated with the minimum target signal $kP_T(\text{min})$, i.e.,

$$S = \frac{kP_T(\text{min})}{\sqrt{\langle n^2 \rangle}} \quad . \tag{44}$$

Suppose that no discriminator is being used, and express the peak detection threshold for target signals as $\varepsilon kP_T(\text{min})$, where $0 < \varepsilon < 1$. Then the probability, P_D, of detecting a minimum target signal is

$$P_D = \frac{1}{2}\left\{1 + \text{erf}\left[\frac{S}{\sqrt{2}}\,(1 - \varepsilon)\right]\right\} \quad . \tag{45}$$

If, instead, we are peak detecting the differentiator-processed signal, then the probability, Q_D, of detecting a minimum target signal is

$$Q_D = \frac{1}{2}\left\{1 + \text{erf}\left[\frac{S}{\sqrt{2}}\,(1 - \bar{\varepsilon})\,\frac{\sqrt{3}}{4TB}\right]\right\} \quad , \tag{46}$$

where the detection threshold is taken as $\bar{\varepsilon}[\pi R_T CkP_T(\text{min})/2T]$, with $0 < \bar{\varepsilon} < 1$. Equation (46) is obtained by integrating equation (33) (with $\langle n^2 \rangle$ replaced by $\langle N^2 \rangle$ and $kP_T(\text{min})$ replaced by $\pi R_T CkP_T(\text{min})/2T$) from the detection threshold to infinity, and by using equations (24) and (44).

Equations (45) and (46) and the equations for P_F can be used to numerically evaluate the discrimination scheme for various specific conditions. For example, suppose that the available signal-to-noise ratio S is 10 to 1 and that the desired single-pulse probability of detecting a minimum target is 0.999. By using the estimate $\sqrt{3}/4TB$ =

0.57, obtained following equation (25), we find from equations (45) and (46) that $\varepsilon = 0.691$ and $\bar{\varepsilon} = 0.458$. Let us take $\rho_0 = 0.1$ and $x_{max} = 10$ m for the minimum target conditions. Let $\sigma_{max} = 0.1\ m^{-1}$, which corresponds to a dense water cloud. For T = 11 ns, figures 7 and 11 give the estimates $F_I = 3.5$ and $m = 2.5 \times 10^{-3}\ \bar{P}_0 A$. For the preprocessing values of x1, x2, and $\bar{B}$, we get $x1 = -0.944/\sqrt{2}$, $x2 = 6.91/\sqrt{2}$, and $\bar{B} = 15.7/\sqrt{2}$. These values lead to $P_F = 0.13$, which would lead to an unacceptably high false-alarm rate if, on the average, only one pulse per mission were returned by an aerosol. For the postprocessing values of x1, x2, and $\bar{B}$, we get $x1 = 1.33/\sqrt{2}$, $x2 = 2.61/\sqrt{2}$, and $\bar{B} = 2.56/\sqrt{2}$. These values lead to $P_F = 0.03$, which is a significant improvement but is still unacceptably high. A similar computation for T = 9 ns gives $P_F = 0.04$ before processing and $P_F = 0.01$ after processing.

The foregoing examples indicate the potential severity of the aerosol problem for the 10-m system considered, and show what level of improvement can be expected from derivative discrimination. For the two cases considered, the single-pulse probability of false alarm after processing is approximately 1/4 that before processing. It should be noted, however, that the method of treating the improvement factor, F_I, in the analysis was such as to underestimate its favorable effect. A more refined analysis should therefore give somewhat better results for the postprocessing P_F. It may also be noted (fig. 7) that for T = 5 ns, the F_I at σ_{max} is roughly twice that for T = 9 and 11 ns. One would therefore expect a greater level of improvement from the discriminator for the 5-ns case. Calculations for the 5-ns case were not done, because the error-function evaluation accuracy needed to compute the corresponding difference in equation (40) could not be readily established for this case using the standard mathematics tables. Such computations could be done readily by computer, if necessary. At any rate, a postprocessing P_F of about 0.001 would be the expected result, and such a value could provide satisfactory aerosol rejection for some systems if multiple-pulse detection logic is used.

2.6 Validity of Aerosol-Return Pulse Model

The basic limitation of the model for calculating aerosol-return signals is that it takes no account of multiple-scattering effects. In general, such effects are negligible for sufficiently low-density aerosols, but the precise low-density range can depend significantly on the beam patterns which characterize the optical transceiver.

The experimental determination of multiple-scattering effects is made difficult by the need for removing the single-scatter intensity from the measurement with fairly high precision. In a great many cases of practical interest, the single-scatter component is dominant, so that a measurement of a small difference between two relatively large numbers

is required. For the backscatter configuration of primary interest for fuzing, use can be made of the differing polarization properties of the single-scatter component as compared to the multiple-scatter component, provided the aerosol consists of approximately spherical particles. For this situation, Mie theory predicts that the single-scatter component retains the polarization of the incident beam, which one can arrange to be highly polarized; on the other hand, the multiple-scatter component will be unpolarized. Indeed, most of the available data (which are sparse) measure the extent of depolarization of the backscattered return for a highly polarized transmitter beam.[5-7,*]

Theoretical calculations of multiple-scattering effects have been considerably more effective and useful than measurements, for most purposes. The calculations are extremely complex, however, and, in their most highly developed form, use Monte Carlo techniques to trace the three-dimensional photon trajectories as they experience multiple-scattering events within the aerosol.

Bird, Blattner, and Collins[2] have developed a Monte Carlo computer code for the investigation of multiple-scattering effects in optical fuze configurations. The code has been subjected to a respectable degree of experimental verification, as well as a comparison of its results with several existing quantitative theories of second-order scattering. Generally, good agreement is seen, although there are discrepancies in some of the theoretical comparisons.[2]

Because multiple-scattering effects can depend significantly on the transceiver optical configuration, especially when the transceiver is near the scattering medium (the situation of most concern with an AOF), it is difficult to form general conclusions which are valid for a wide class of systems. Case-by-case evaluation thus seems indicated; however, an alternative might be an ambitious exploration of multiple-scattering effects in various generic optical configurations, using the Bird-Blattner-Collins computer code.

---

[2]*R. E. Bird, Calculations of Multiple-Scattering Effects on Active Optical Sensors in Cloud Environments, Naval Weapons Center, NWC TP 5667 (August 1974).*

[5]*E. Reisman and J. Pope, Final Report, Laser Polarization Scattering Studies, prepared by Philco-Ford Corp., under contract No. N00123-72-0244, for Naval Weapons Center (November 1972).*

[6]*J. Manz, A Ladar Cloud/Target Polarization Discrimination Technique, Air Force Systems Command, AFWL-TR-70-76 (October 1970).*

[7]*Z. G. Sztankay and D. W. McGuire, Backscatter in Clouds at 0.9 μm and its Effects on Optical Fuzing Systems, Proc. of Seventh DoD Conference on Laser Technology (November 1977).*

**D. A. Giglio discusses multiple scattering in a fuzing context in an internal HDL report R-930-74-2, January 1974, entitled Some Comments on Multiple Scattering in Aerosols and the Depolarization of Backscattered Light.*

At the request of HDL, Bird has exercised the Monte Carlo code to determine the effects of multiple scattering for a system configuration similar to that used to evaluate derivative discrimination (sect. 2.3). In what follows, the results of this analysis are highlighted.

The system configuration analyzed used uniform pencil beams which were fully overlapped from 3.5 m to infinity and partially overlapped between 2.0 and 3.5 m. The transmitter output (0.9-µm wavelength) was variously taken to be cw or pulsed; when pulsed, both rectangular and half-sine-wave pulse shapes were used; the pulse widths (FWHM) employed were 6.5 and 9.0 ns. For an aerosol model, the well-known Deirmendjian model C_1 fair-weather cumulus cloud was selected.[8]

Several aspects of the multiple-scattering effects that occur were investigated as a function of the extinction level. For a cw source, the relative contributions of the first three orders of scattering to the total were calculated for $0.01\ m^{-1} \leq \sigma \leq 0.3\ m^{-1}$. These results are summarized in figure 13, which plots the total received backscatter and the contributions just mentioned versus σ. Calculations of the return pulse shapes for the several pulsed cases were also performed, and the resulting pulse widths (FWHM) were compared with those obtained from single-scatter calculations. Very little difference was observed in this comparison. In addition to calculating return pulse shapes, the depolarization characteristics of the received pulses were determined assuming a linearly polarized transmitter output. This was done by calculating both the total return and that part of it polarized perpendicularly to the transmitter polarization direction. The cross-polarized return ranged from approximately 3 to 20 percent of the total as σ ranged from 0.05 to 0.3 m^{-1}, indicating a generally significant multiple-scatter component in spite of the negligible effect on the pulse width.

The results shown in figure 13, together with the results on the cross-polarized returns, show that multiple-scattering effects become significant in the system analyzed for extinction coefficients of around 0.1 m^{-1}. However, the results connected with return pulse widths suggest that multiple scattering may not play much of a role in determining pulse shapes.

---

[8]D. Deirmendjian, *Electromagnetic Scattering on Spherical Polydispersions*, American Elsevier Publishing Co. (1969).

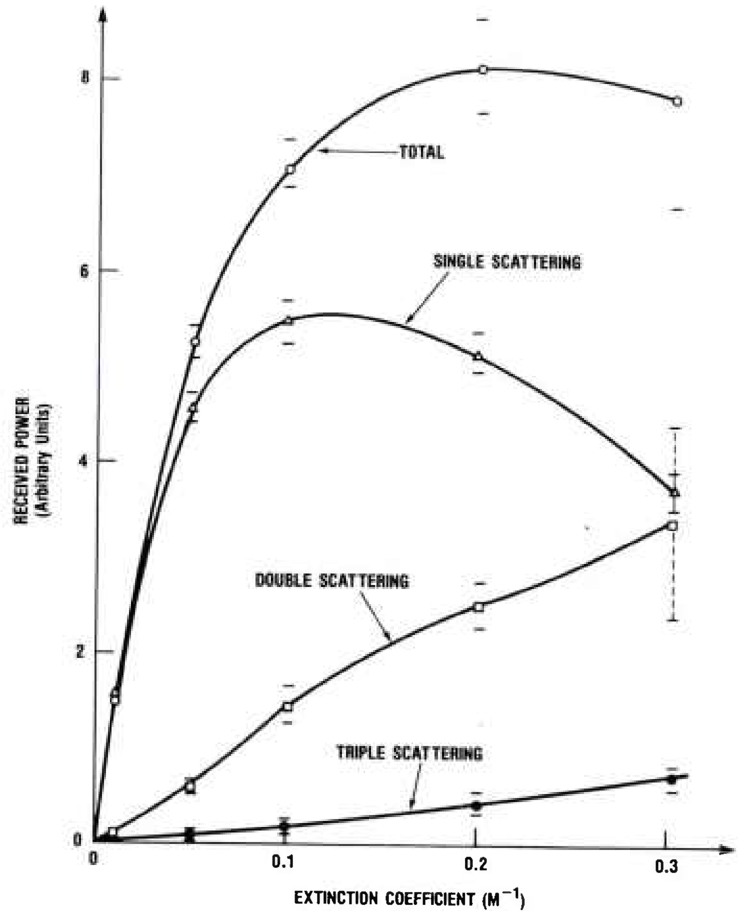

Figure 13. Total received backscattered power and contributions from first three orders of scattering versus extinction coefficient for a 0.9-μm continuous-wave pencil-beam active optical-detection system fully immersed in a uniform Deirmendjian model C_1 fair-weather cumulus cloud (curves calculated using Monte Carlo multiple-scattering computer code; error bars indicate standard deviations of computations).

Another view can be taken of the validity of the aerosol-pulse return model used for the derivative discrimination analysis. If the model can accurately replicate the shapes of actual measured aerosol-return signals, then it is certainly a useful tool for analyzing pulse-shape discrimination techniques. To see how to achieve the desired replication, consider equations (9) and (10). After having chosen functions P(t) and R(x) to model the transmitter pulse shape and range response of the AOF, one then seeks to find functions $\sigma(x)$ and $\mu(x)$ that make the computed return signal (from eq (10)) fit the measured return signal. If the model described by equations (9) and (10) is accurate,

then the foregoing procedure will lead to a good fit of the measured signal, with $\sigma(x)$ and $\mu(x)$ being the actual extinction and backscatter profiles of the aerosol.

The fitting procedure just described, athough in general difficult to carry out, becomes a relatively simple two-parameter fitting problem, if the aerosol is assumed to be uniform over the extent of the system's influence pattern. Then μ and σ are constants, and the problem is to find values for them that minimize, say in a least-square sense, the difference between $V(t)$ in equation (10) and the measured return signal. It is, of course, assumed that the measured signal was returned by a uniform aerosol.

To evaluate the return pulse model along the foregoing lines, 10 samples of measured fair-weather cumulus cloud-return signals were selected from an HDL data collection using the following criteria:

a. The measured return signals should correspond to full immersion of the measurement system in uniform aerosol.

b. The extinction levels (σ-values) of the clouds for the selected sample should span a wide range, including both low- and high-density clouds.

The measurements in question were made by HDL personnel during instrumented helicopter flight tests through water clouds. Two separate instruments were used to collect the data. A pulsed GaAs laser probe furnished the pulse return measurements, and a dual-channel nephelometer, using a filtered xenon arc-lamp source, provided an independent characterization of the cloud environment by measuring the extinction and backscatter coefficients. This measurement program is discussed in detail by McGuire, Smalley, and Sztankay.[9] The nephelometer measurements are valid only when the cloud being measured is uniform over the region probed by the nephelometer beams, a region roughly the same as that probed by the GaAs laser pulser. Several operational criteria are applied to the raw nephelometer data to validate cloud uniformity; although not foolproof, these criteria are considered generally reliable. A detailed description of the use of the nephelometer for cloud measurements, including some data analysis and validation, is given by Giglio, Rod, and Smalley.[10]

---

[9]*D. W. McGuire, H. M. Smalley, and Z. G. Sztankay, Measurements of Backscatter Effects in Clouds at 0.9 μm, Proc. of JTCG/MD/WPFF Tri-Service Optical Fuze Technology Symposium (October 1976).*

[10]*D. A. Giglio, B. J. Rod, and H. M. Smalley, Nephelometer Mapping of Backscatter and Attenuation Coefficients of Clouds, Harry Diamond Laboratories, HDL-TR-1660 (February 1974).*

The 10 sample return signals were then subjected to a weighted least-square fitting procedure, using the aerosol-return pulse model and assuming cloud uniformity. The squared deviations of the theoretical pulse from the measured pulse were weighted by the value of the measured signal. This procedure tends to make the theoretical pulse fit the measured one better where the signal level is high, thus deemphasizing the effect of measurement noise. Typical results are shown in figures 14 through 16. The solid curves in these figures are the best-fit model pulses, while the dots show the sampled values of the measured return used in the fitting procedure. The quality of the fits can be seen to be quite good. Figure 16 shows the least impressive fit obtained (provided that results with two of the sample pulses, which were found to actually have been produced by decidedly nonuniform cloud distributions, are not considered).

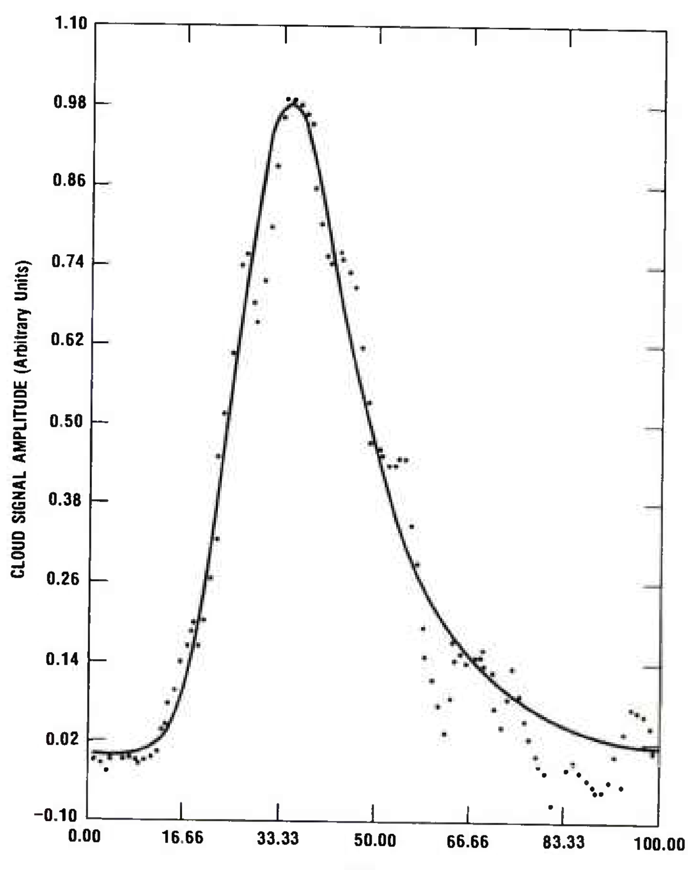

Figure 14. Sampled values of measured cloud-return pulse (dots) and weighted (by sample values) least-squares fit (solid curve) according to equations (9) and (10) for a uniform cloud (measured cloud pulse sample No. 1).

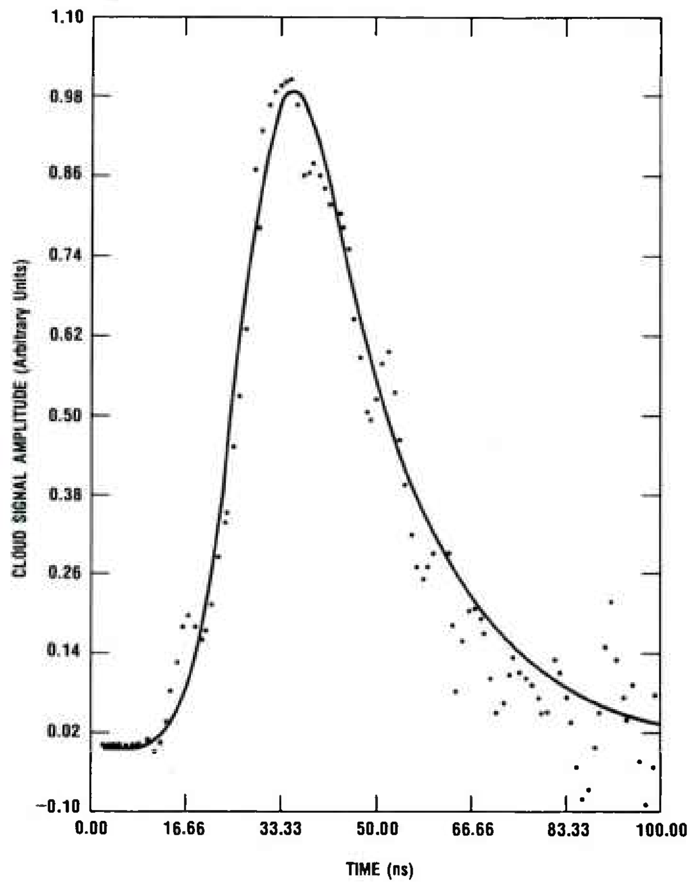

Figure 15. Sampled values of a measured cloud-return pulse (dots) and weighted (by sample values) least squares fit (solid curve) according to equations (9) and (10) for a uniform cloud (measured cloud pulse sample No. 6).

A disturbing feature of the foregoing results is that the best-fit extinction coefficients are consistently lower (by about a factor of 2.5) than those given by the nephelometer. A possible explanation for the discrepancy lies in the fact that the received cloud signals obtained with the laser probe are only approximately due to direct backscatter. Because of the finite separation between the transmitter and receiver (typically about 7 cm), the received power arises from scattering over a small range of angles near the backscatter direction. Since the cloud scattering function (the ratio of the volume scattering coefficient as a function of angle to the extinction coefficient) can vary substantially with angle near the backscatter direction, it may be that the discrepancy in question is due to the simple inter

pretation given to the shape of the cloud-return pulse, namely, that it results from direct backscatter with no variation in the scattering function. Further discussion of this question will be given in a future publication, where the fitting procedure and all the results obtained with it will be described in detail.

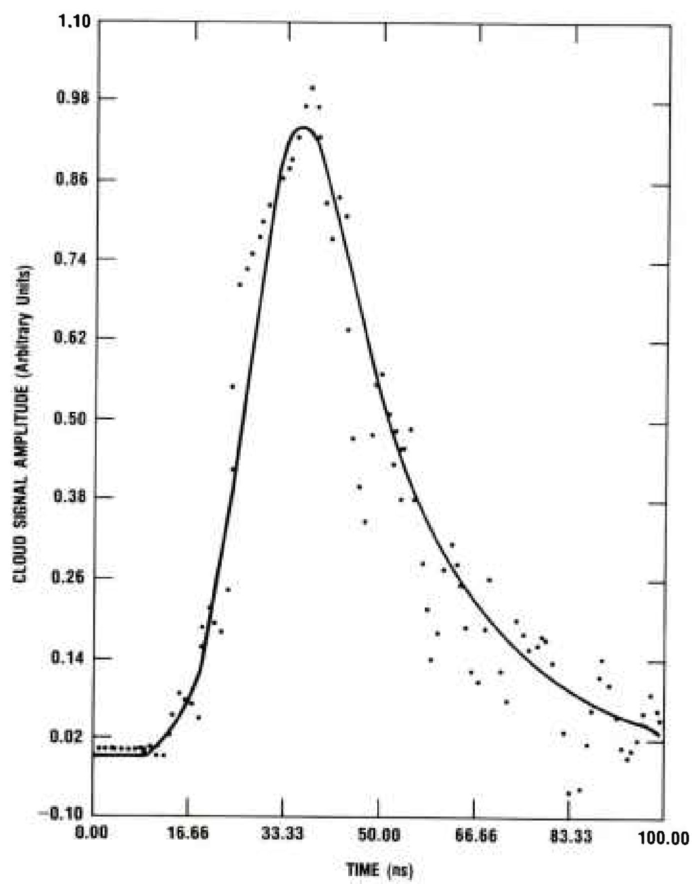

Figure 16. Sampled values of a measured cloud-return pulse (dots) and weighted (by sample values) least-squares fit (solid curve) according to equations (9) and (10) for a uniform cloud (measured cloud pulse sample No. 7).

3. DERIVATIVE DISCRIMINATION APPLIED TO MEASURED CLOUD-RETURN PULSES

A main objective of the overall research on aerosol discrimination techniques is to use the growing HDL data bank of measured aerosol-return signals to evaluate discrimination schemes directly. Now that the capability has been developed for automatically processing and

analyzing such data with a computer, it will be possible to realize this objective. As an illustration of the kinds of evaluation we are speaking of, this section and the next evaluate derivative discrimination and a low-pass filter scheme, respectively, using the measured cloud-return pulses that were considered in section 2.6 for the validation of the aerosol-return pulse model. Only the eight return signals which were found to be well-modeled (from the standpoint of pulse shape) by equations (9) and (10) for a uniform aerosol distribution were considered for these evaluations.

The eight cloud-return pulses and eight simulated target-return signals were differentiated and then low-pass filtered at various bandwidths to simulate the bandpass characteristics of potential receiver amplifiers. This was done numerically with a computer using digitized representations of the signals. The upper-frequency cutoffs (defined as the frequency at which the filter's response is 3 dB down) used were 17.5, 35, and 52.5 MHz, and the filters were digital simulations of the simple single-pole type. The target signals were chosen to have the same amplitude as the corresponding cloud returns, and to have the shape shown in figure 17, which was obtained from an accurate measurement of the shape of the transmitter pulse of the laser probe used to obtain the cloud-return pulses.* A random number generator was used to simulate target-signal noise. The noise bandwidth and rms noise level were arranged to be approximately the same as for the cloud-return signals. (The noise bandwidth was about 200 MHz and the typical SNR was about 15:1.)

Examples of the processed signals are shown in figures 18 through 23. A complete summary of the peak values of these signals is given in table 2. Both the positive- and negative-going peaks are compared, and the ratios of the target peaks to the corresponding cloud peaks are given. Although indicative of target/cloud contrast improvement, the ratios do not give the contrast-improvement factor F_I defined in section 2.3, because F_I is independent of the noise levels. We also give, in the last two columns of the table, the extinction levels associated with the cloud-return pulses. Notice the previously mentioned difference between the measured extinction coefficients (as determined in flight with a nephelometer) and those determined by curve fitting the measured return pulse with a uniform cloud model via equations (9) and (10).

**The shape referred to is that which is seen at the output of the probe's receiver amplifier upon reflecting the transmitter pulse from a standard target.*

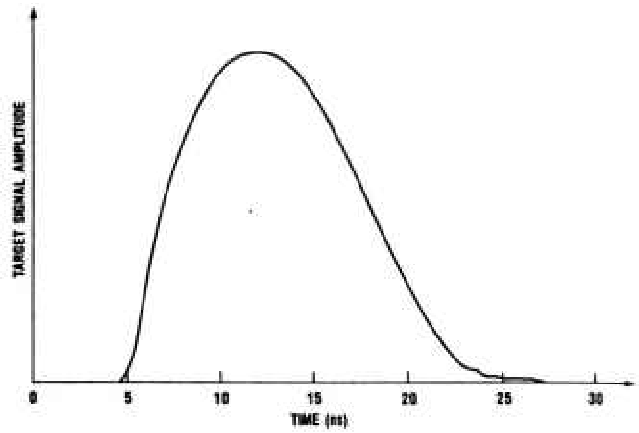

Figure 17. Temporal shape of target signals chosen for analysis in section 3.

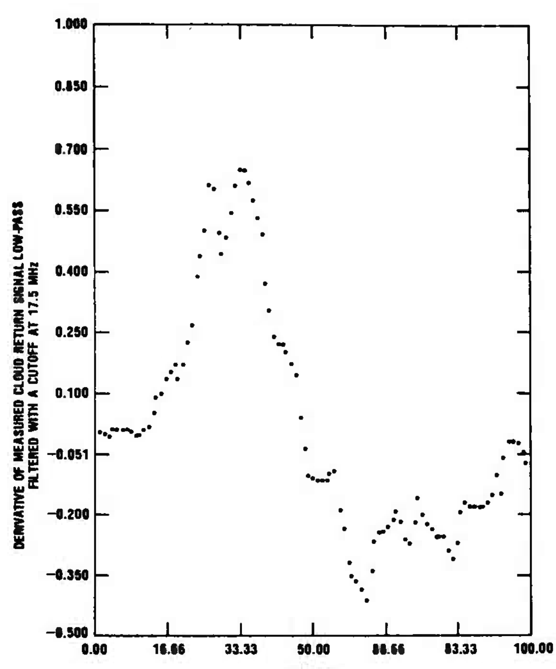

Figure 18. Filtered derivative of measured cloud-return signal (sample No. 1) . Filter is of low-pass single-pole type with 17.5-MHz cutoff frequency.

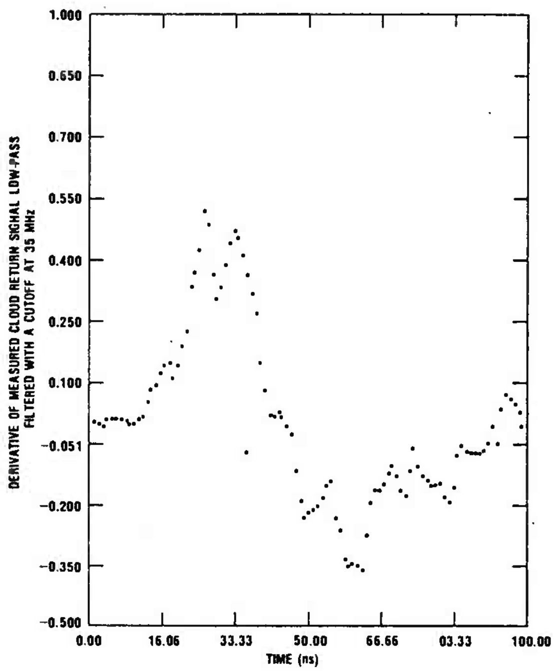

Figure 19. Filtered derivative of measured cloud-return signal (sample No. 1). Filter is of low-pass single-pole type with 35-MHz cutoff frequency.

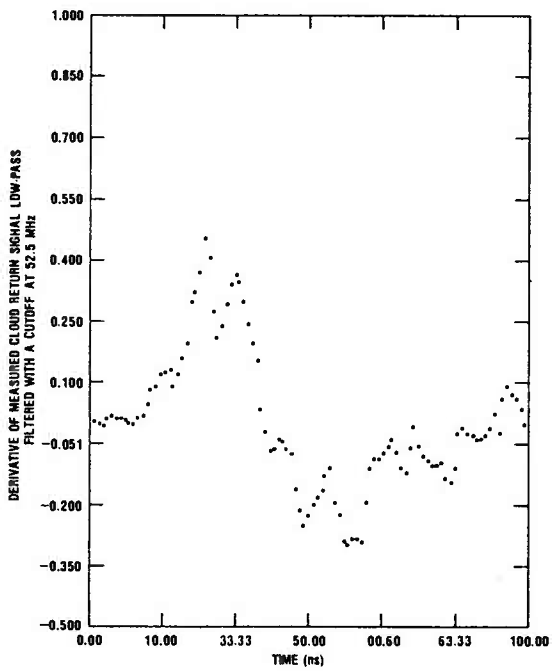

Figure 20. Filtered derivative of measured cloud-return signal (sample No. 1). Filter is of low-pass single-pole type with 52.5-MHz cutoff frequency.

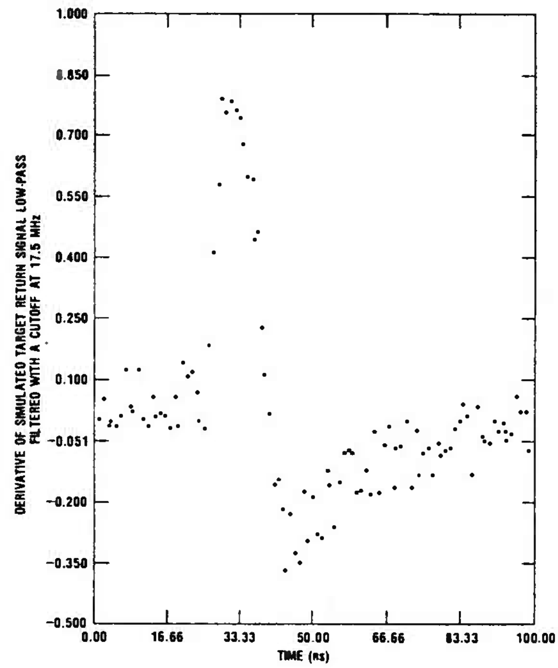

Figure 21. Filtered derivative of simulated target signal whose peak amplitude equals that of cloud-return sample No. 1. Filter is of low-pass single-pole type with 17.5-MHz cutoff frequency.

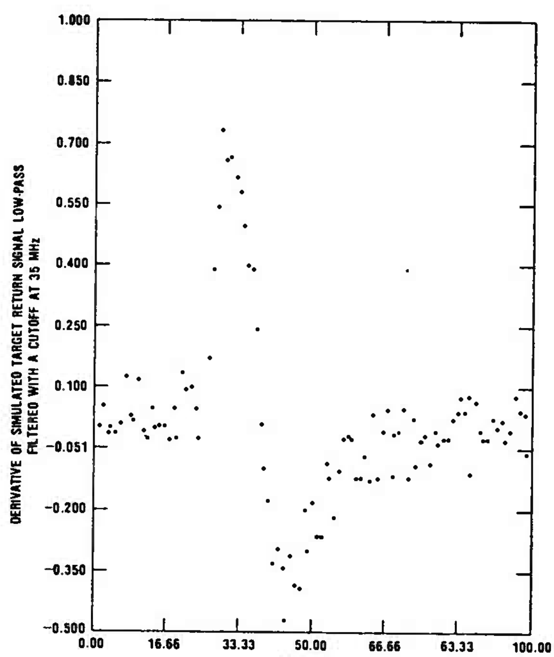

Figure 22. Filtered derivative of simulated target signal whose peak amplitude equals that of cloud-return sample No. 1. Filter is of low-pass single-pole type with 35-MHz cutoff frequency.

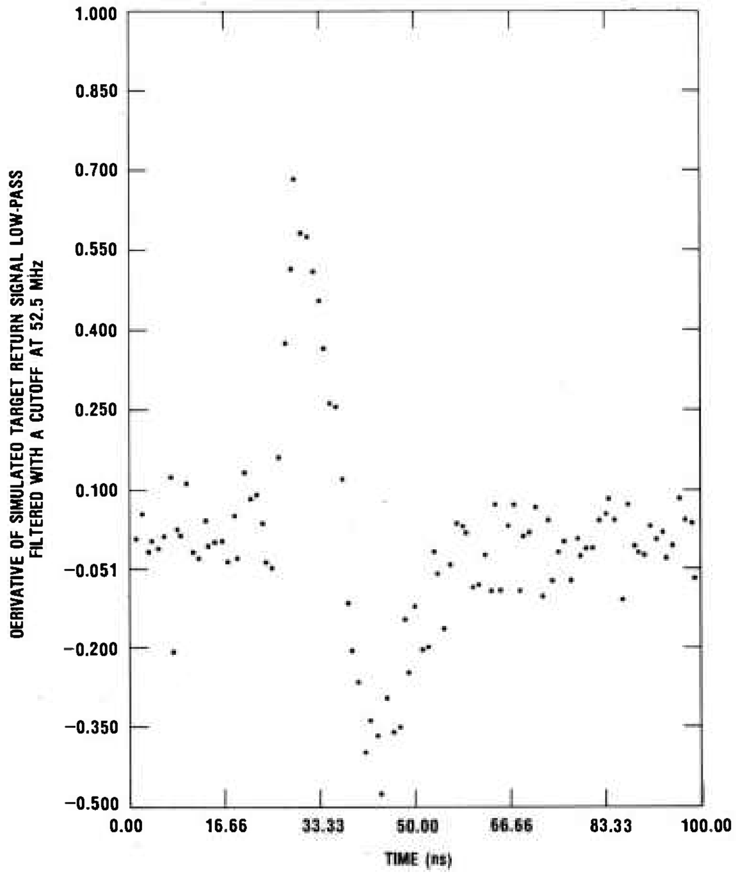

Figure 23. Filtered derivative of simulated target signal whose peak amplitude equals that of cloud-return sample No. 1. Filter is of low-pass single-pole type with 52.5 MHz cutoff frequency.

TABLE 2. RESULTS OF DERIVATIVE PROCESSING OF A SAMPLE OF MEASURED CUMULUS CLOUD-RETURN SIGNALS AND SIMULATED TARGET-RETURN SIGNALS

Filter cutoff (MHz)	Cloud pulse No.	Cloud peak (+)	Target peak (+)	Target/cloud ratio	Cloud peak (-)	Target peak (-)	Target/cloud ratio	Measured extinction $\sigma(m^{-1})$	Curve fit extinction $\sigma(m^{-1})$
52.5	1	0.450	0.678	1.51	0.295	0.479	1.62	0.25	0.11
	2	0.372	0.618	1.66	0.301	0.381	1.27	0.21	0.06
	4	0.324	0.686	2.12	0.294	0.467	1.59	0.16	0.08
	5	0.398	0.601	1.51	0.227	0.406	1.79	0.22	0.02
	6	0.485	0.721	1.49	0.274	0.478	1.74	0.14	0.06
	7	0.521	0.741	1.42	0.351	0.445	1.27	0.13	0.06
	8	0.499	0.819	1.64	0.360	0.573	1.59	0.17	0.09
	10	0.432	0.722	1.67	0.310	0.542	1.75	0.21	0.06
35	1	0.517	0.726	1.40	0.363	0.474	1.31	Same	Same
	2	0.451	0.658	1.46	0.342	0.393	1.15		
	4	0.410	0.734	1.79	0.337	0.443	1.31		
	5	0.483	0.641	1.33	0.266	0.383	1.44		
	6	0.571	0.787	1.38	0.335	0.455	1.36		
	7	0.566	0.811	1.43	0.349	0.458	1.31		
	8	0.554	0.928	1.68	0.437	0.535	1.22		
	10	0.537	0.817	1.52	0.351	0.523	1.49		
17.5	1	0.647	0.790	1.22	0.413	0.367	0.89	Same	Same
	2	0.583	0.754	1.29	0.334	0.322	0.96		
	4	0.579	0.826	1.43	0.353	0.369	1.05		
	5	0.618	0.728	1.18	0.269	0.304	1.13		
	6	0.711	0.862	1.21	0.380	0.357	0.94		
	7	0.627	0.888	1.42	0.349	0.398	1.14		
	8	0.766	1.08	1.41	0.472	0.432	0.92		
	10	0.715	0.919	1.29	0.371	0.407	1.10		

Several features of the tabulated results should be noted. First, there is a general decline in the target/cloud ratio as the filter cutoff frequency diminishes from 52.5 to 17.5 MHz, with virtually all contrast improvement vanishing at 17.5 MHz for the negative-going peaks. This occurs because the relative speed difference between the target and cloud pulses tends to disappear as the reception bandwidth decreases. Increasing the bandwidth beyond 52.5 MHz (which should be feasible since good quality photodetector-amplifier combinations with 150-MHz bandwidths have been developed) should give better contrast ratios; however, the consequent increased effect of noise would then cause greater scatter in the results. The reader has probably noticed that there is no general superiority in the contrast ratios for the negative-going peaks; in fact, there is indication of the opposite, especially for the 17.5-MHz results. This occurs because the transmitted (and assumed target return) pulse is asymmetrical, having a faster leading than trailing edge. Finally, if the target/cloud ratio is plotted versus the extinction level, one finds no discernible correlation between the two. The four possible plots of this kind for the 52.5-MHz results are shown in figure 24. Although one would expect to find a correlation indicating greater contrast ratios for lower extinction levels, it may be that for the range of extinction levels concerned the F_I-versus-σ curve shows little variation (see, for example, fig. 7).

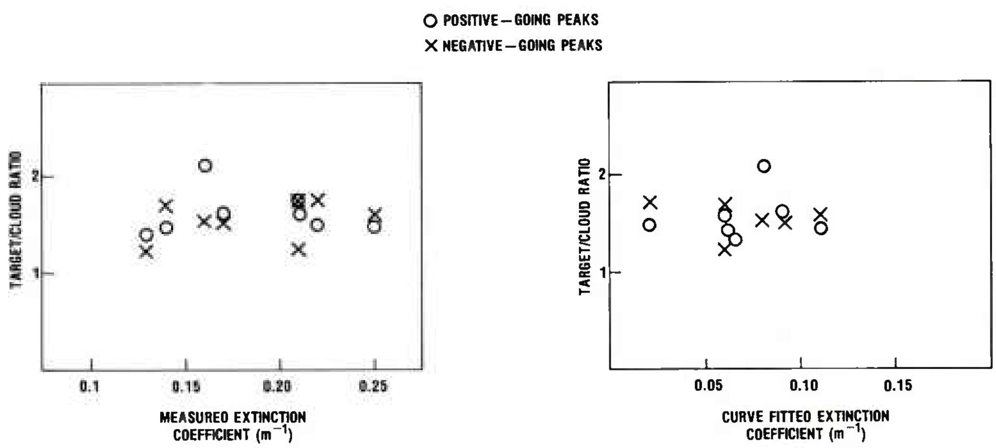

Figure 24. Plots of target/cloud peak signal ratios given in table 2 versus corresponding measured and curve-fitted extinction coefficients, for 52.5-MHz filter cutoff case.

To analyze the performance of a fuze system that functions in response to a threshold crossing, one wants to determine, for a given threshold level, the probabilities of (a) functioning in response to a cloud signal and (b) failing to function on a legitimate target signal. These probabilities can be determined from the distribution of cloud and target signals about their respective means. Were the data in table 2 of statistically significant proportions, the needed probability distributions could be estimated reasonably accurately with standard statistical methods. Since our data sample is so small, we have chosen as a computational expedient to assume that the peak target and cloud signals are normally distributed about their means.

For each filter cutoff, the means and variances of the four categories of peak signals were estimated in the standard manner. The results are given in table 3. Let μ_1 and Σ_1^2 denote the mean and variance of a particular group of peak cloud signals, and let μ_2 and Σ_2^2 denote the like quantities for the corresponding group of peak target signals. If the threshold T is set by

$$T = \frac{\mu_1 \Sigma_2 + \mu_2 \Sigma_1}{\Sigma_1 + \Sigma_2} \tag{47}$$

then functioning on a cloud and failing to function on a target will be equally probable. These probabilities were computed from the data in table 3, and the results are given in table 4.

TABLE 3. ESTIMATED MEANS AND VARIANCES OF VARIOUS GROUPS OF CLOUD AND TARGET SIGNAL PEAKS FROM TABLE 2 VERSUS FILTER CUTOFF FREQUENCY

Filter cutoff (MHz)	Cloud signal peak				Target signal peak			
	Positive peak		Negative peak		Positive peak		Negative peak	
	Mean	Variance	Mean	Variance	Mean	Variance	Mean	Variance
52.5	0.435	0.00398	-0.302	0.00159	0.698	0.00424	-0.472	0.00358
35	0.511	0.00298	-0.347	0.00190	0.763	0.00762	-0.458	0.00251
17.5	0.656	0.00403	-0.367	0.00308	0.856	0.01080	-0.370	0.00159

TABLE 4. PROBABILITY OF FAILURE VERSUS FILTER CUTOFF FREQUENCY[a]

Filter cutoff (MHz)	Probability of failure	
	Positive peak	Negative peak
52.5	0.02	0.045
35	0.038	0.19
17.5	0.12	0.5

[a] *Failure = functioning on a cloud = missing a target. Values calculated from data in table 3.*

The foregoing analysis should be considered only as illustrative of how a large, statistically significant data sample would be analyzed. To the extent that the results in table 4 can be taken seriously, it must be admitted that at their best (52.5-MHz filter cutoff) they are unspectacular. Spectacular improvement in target/cloud contrast is not, however, predicted theoretically for the relatively broad 11-ns transmitter pulse considered in the evaluation; decidedly better results are expected for narrower pulses of around 5-ns FWHM, and also especially for pulses with faster falling edges.

A fully realistic evaluation would have to consider overall mission probabilities of false alarm, which would require an accounting of the probabilities of receiving sequences of cloud pulses. While such accounting would place further demands on the single-pulse false-alarm probability, the use of multiple-pulse detection logic, if consistent with the desired probability of detection, could significantly improve the overall picture.

4. A LOW-PASS FILTER DISCRIMINATION SCHEME APPLIED TO MEASURED CLOUD-RETURN PULSES

The basic idea of the low-pass filter method to be considered is as follows. All received signals are first subjected to a threshold test which rejects those signals with amplitude below some level determined by minimum detectable target conditions. If the signal is not rejected, it is normalized to some convenient fixed amplitude and low-pass filtered. The filtering results in the approximate integration of the normalized signal, so that relatively wide pulses give higher filter outputs than narrower ones. A second threshold test is then performed that rejects peak filter outputs above some level between the mean levels for legitimate targets and clouds. A signal not rejected at this stage is considered a legitimate target return and the firing sequence is initiated.

The foregoing scheme is essentially the inverse of derivative discrimination. Since signal integration is a smoothing process, it is expected that noise will have a smaller effect in the second threshold test than it does in derivative discrimination. However, two threshold test performed in sequence are required in the low-pass scheme, and the first one cannot be avoided because without it there would be a very high probability of firing on narrow, low-level noise pulses. Thus, overall probabilities of detection and false alarm will be determined by the series combination of possible detection errors in both threshold tests, and noise performance comparisons of derivative and low-pass filter discrimination must be made in view of this.

The main question of implementability with the low-pass scheme lies in the signal normalization function. Good signal integrators could be made easily and cheaply with a simple resistor/capacitor combination whose time constant is large compared to the signal pulse width. It would be relatively easy to implement a crude version of signal normalization, namely, clipping at a predetermined level. Such an approach could have difficulty with large-amplitude target pulses having a large base width; however, this difficulty might be overcome by introducing a relatively high-level threshold test to identify large-amplitude target signals. Better quality signal normalization might be achieved with an amplifier whose gain could be controlled by an external signal. Such an amplifier and a delay device could be placed at the input to the integration channel. By then using fast peak detection in a parallel channel, a gain-control signal could be developed that might also be used for the first threshold test. This alternative will be investigated.

As a preliminary test of the low-pass method, the method was applied to the measured cloud returns and corresponding simulated target signals used for the similar test of derivative discrimination (sect. 3). The normalized signals were passed through several single-pole low-pass filters (cutoffs at 17.5, 12.5, and 7 MHz), and the peak values of the filter outputs were noted. Typical waveforms of the filter outputs are shown in figures 25 though 30. A summary of the peak values and contrast ratios is given in table 5.

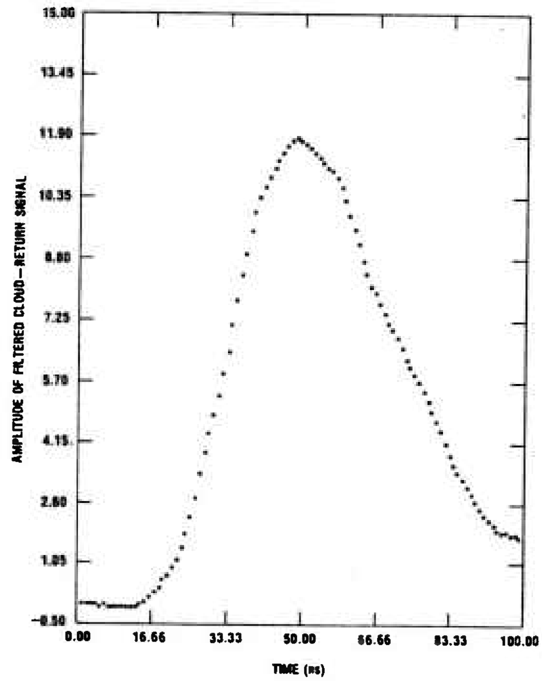

Figure 25. Cloud-return signal, sample No. 1, after passing through 17.5-MHz single-pole low-pass filter.

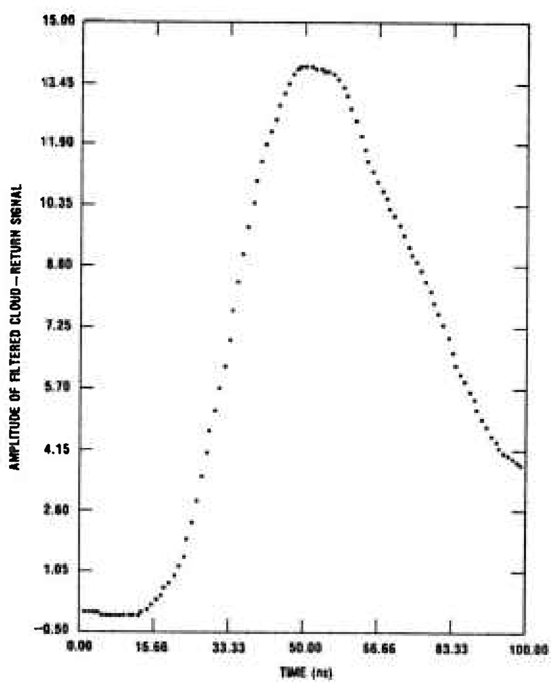

Figure 26. Cloud-return signal, sample No. 1, after passing through 12.5-MHz single-pole low-pass filter.

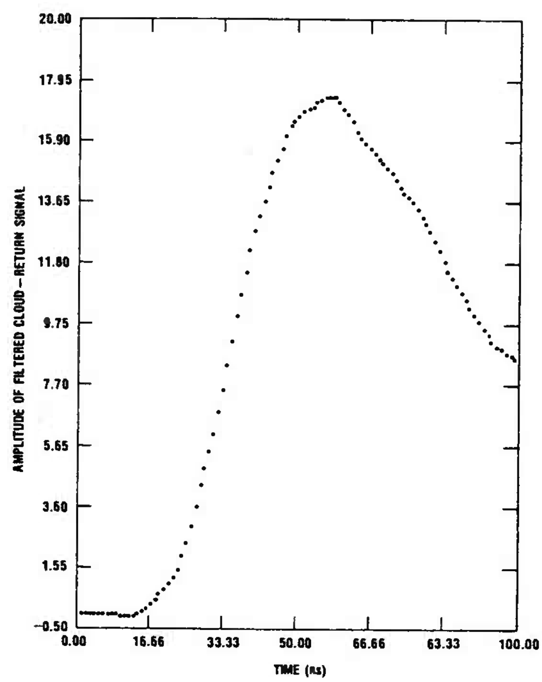

Figure 27. Cloud-return signal, sample No. 1, after passing though 7-MHz single-pole low-pass filter.

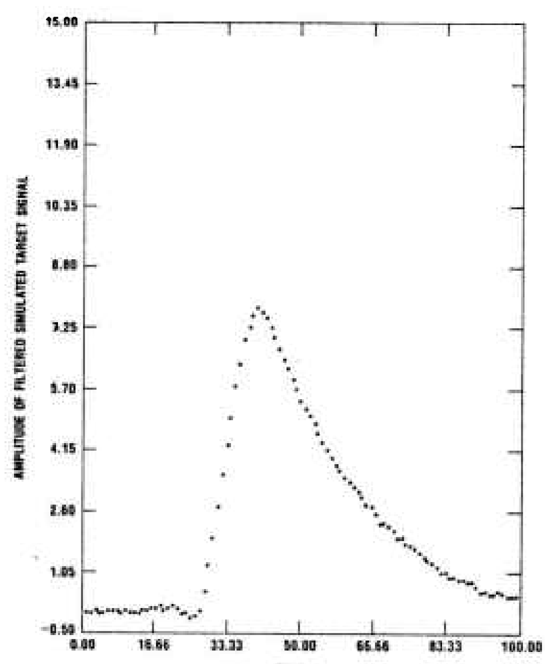

Figure 28. Simulated target signal (whose peak amplitude equals that of cloud return sample No. 1) after passing through 17.5-MHz single-pole low-pass filter.

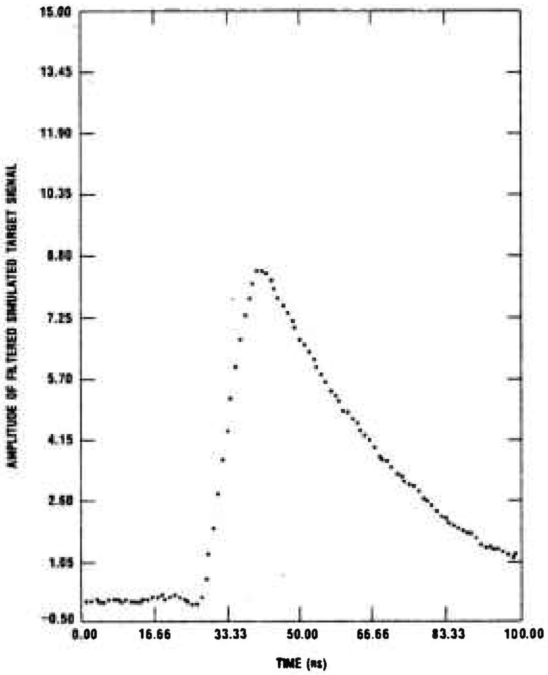

Figure 29. Simulated target signal (whose peak amplitude equals that of cloud return sample No. 1) after passing through 12.5-MHz single-pole low-pass filer.

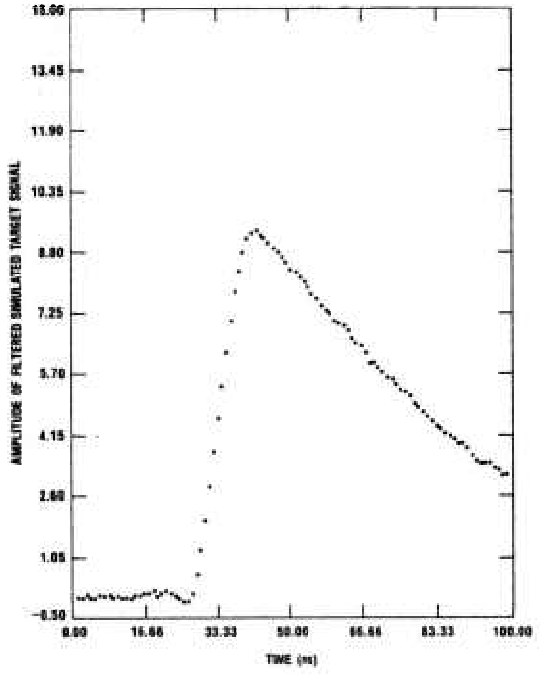

Figure 30. Simulated target signal (whose peak amplitude equals that of cloud return sample No. 1) after passing though 7-MHz single-pole low-pass filter.

TABLE 5. RESULTS OF APPLYING THE LOW-PASS FILTER DISCRIMINATION SCHEME TO MEASURED CUMULUS CLOUD-RETURN SIGNALS AND SIMULATED TARGET-RETURN SIGNALS

Compared are the peak filter outputs for cloud and target signals versus the filter cutoff frequency

Filter cutoff (MHz)	Cloud pulse No.	Cloud peak	Target peak	Cloud/target ratio
17.5	1	11.8	7.72	1.53
	2	9.51	6.68	1.42
	4	11.4	7.90	1.44
	5	11.0	6.96	1.58
	6	12.0	8.10	1.48
	7	11.4	7.88	1.45
	8	14.2	9.16	1.55
	10	13.1	8.48	1.54
12.5	1	13.9	8.39	1.66
	2	11.2	7.32	1.53
	4	13.6	8.66	1.57
	5	13.0	7.66	1.70
	6	14.3	8.93	1.60
	7	13.2	8.66	1.52
	8	16.7	10.0	1.67
	10	15.6	9.38	1.66
7	1	17.4	9.33	1.86
	2	14.0	8.06	1.74
	4	17.0	9.66	1.76
	5	16.5	8.49	1.94
	6	17.9	9.95	1.80
	7	16.8	9.52	1.76
	8	20.5	11.1	1.85
	10	19.4	10.5	1.85

The contrast ratios are roughly the same as obtained with the derivative method (but the ratio is inverted), and there is a consistent improvement in the contrast as the cutoff frequency diminishes. As with the derivative scheme, the probabilities of failure to distinguish between targets and clouds can be determined by assuming normal statistics and estimating the means and variances for the target and cloud signal distributions. The estimates are given in table 6, and the ratios of the means to the square roots of the variances are indicated, these giving a kind of signal-to-noise ratio. The latter are seen to be roughly constant versus the filter cutoff frequency when targets and clouds are considered separately; there is little variation even when target and cloud data are considered together. If a threshold is set in accordance with equation (47), the two types of failure probability are again equal. These are given for the several cutoff frequencies in table 7. Note again that only single-pulse probabilities are given.

TABLE 6. ESTIMATED MEANS AND VARIANCES OF LOW-PASS FILTERED CLOUD AND TARGET SIGNAL PEAKS FROM TABLE 5 VERSUS FILTER CUTOFF FREQUENCY

Filter cutoff (MHz)	Cloud signal peaks			Target signal peaks		
	Mean	Variance	Mean/$\sqrt{\text{variance}}$	Mean	Variance	Mean/$\sqrt{\text{variance}}$
17.5	11.8	1.72	9.01	7.86	0.546	10.6
12.5	13.9	2.46	8.85	8.63	0.654	10.7
7	17.4	3.42	9.41	9.57	0.848	10.4

TABLE 7. PROBABILITY OF FAILURE VERSUS FILTER CUTOFF FREQUENCY CALCULATED FROM DATA IN TABLE 6

Filter cutoff (MHz)	Probability of failure
17.5	0.0256
12.5	0.0126
7	0.0023

The failure probabilities indicated in table 7, although still not spectacular, are about an order of magnitude better than those obtained in section 3 for the derivative scheme. The potentiality for further improvement can be partially analyzed using the easily derived relationship

$$\bar{P}_F(f) = \frac{1}{2}\left[1 - \mathrm{erf}\left(\frac{1}{\sqrt{2}}\,\frac{R_c(f) - 1}{\lambda_2 + \lambda_1 R_c(f)}\right)\right] \quad , \tag{48}$$

which gives the failure probability $\bar{P}_F$ for cutoff frequency f in terms of the contrast ratio $R_c(f)$ (as a function of the cutoff frequency) and the approximately frequency-independent ratios $\lambda_1 = \Sigma_1/\mu_1$ and $\lambda_2 = \Sigma_2/\mu_2$; erf denotes the standard Gaussian error function. Since erf monotonically increases from zero and tends asymptotically to unity as its argument runs from zero to $+\infty$, the failure probability is a strictly decreasing function of $(R_c - 1)/(\lambda_2 + \lambda_1 R_c)$. Moreover, since

$$\frac{d}{dR_c}\,\frac{R_c - 1}{\lambda_2 + \lambda_1 R_c} = \frac{\lambda_1 + \lambda_2}{(\lambda_2 + \lambda_1 R_c)^2} > 0 \quad , \tag{49}$$

for all values of the contrast ratio, it follows that $\bar{P}_F$ is a strictly decreasing function of R_c. Thus, the minimum achievable failure probability will occur when $R_c(f)$ is maximum as a function of f. To apply this result to a frequency range bigger than the 7 to 17.5 MHz range used in the computations, one must assume that λ_1 and λ_2 continue to be approximately frequency-independent in the larger range. If this assumption is correct, then the unequivocal trend to higher contrast ratios as the cutoff frequency decreases (table 5) shows the potential for improvement. Were a contrast ratio of 2 achievable, the failure probability would be 0.00075, which would be acceptable for some systems if multiple-pulse detection logic could be used. If a 2.5 contrast ratio could be reached, the probability of failure would be down to 0.00005.

In judging the significance of the foregoing, the size of the data sample and the assumptions made in the analysis (e.g., normal statistics) must be remembered. Also not to be forgotten are the error probabilities associated with the first threshold test of the discrimination scheme. If the potentiality for improvement connected with using less simple low-pass filter characteristics is added to the picture, we judge that the discrimination scheme is sufficiently promising to warrant further investigation. There is a significant difference between this scheme and the derivative discriminator: while the derivative discriminator would fail to properly identify an aerosol signal if its amplitude were too high, the low-pass scheme, which basically senses pulse width, works essentially independently of aerosol (and target) signal levels.

5. SUMMARY AND DISCUSSION

Both aerosol discrimination techniques discussed in this report have potential usefulness for aerosol-resistant optical fuze systems, as indicated by the evaluations presented. The evaluations were, however, limited to pencil-beam influence pattern systems. Such systems are of interest mainly for ground-target applications, although azimuthally sweeping a pencil beam could provide an approach to air-target applications, where 360-deg coverage of the target space is ordinarily required.

For the derivative technique (that is, processing received signals with an RC-differentiator circuit), the general area of system applicability is indicated by the analytical and numerical results presented in this report. Systems that have only a marginal aerosol problem, because of a combination of moderate desired detection ranges and not too severe expected aerosol environments, can be made to effectively reject aerosol signals by using a derivative discriminator and sufficiently short transmitter pulses (on the order of 5-ns wide). Care must be taken in

the design to ensure a relatively high preprocessing SNR, however, because the derivative discriminator will always degrade the SNR. This report discusses the general methods and gives many of the specific analyses needed to design and evaluate such a system. Some further validation of the analysis through comparison with experimentally measured aerosol-return signals is needed and planned.

The low-pass filter scheme discussed, which consists of initial threshold detection followed by signal normalization to a predetermined fixed amplitude, subsequent low-pass filtering, and a final threshold detection, is judged to be superior in several respects to the derivative technique, in spite of the preliminary nature of the evaluation given to the scheme. The low-pass filter scheme is inherently superior from a noise standpoint, since the process tends to smooth received signals. The scheme is also essentially independent of the absolute levels of aerosol and target signals, and therefore could provide effective discrimination in severe aerosol environments. Moreover, the scheme is inherently less sensitive, compared with the derivative technique, to changes in return-signal pulse shape that do not significantly alter the overall pulse width, because the filter is essentially integrating a normalized pulse, and so is sensing pulse width. For the derivative technique, any alteration of pulse shape that affects the maximum slope on the leading or trailing edge, whichever is being detected, will directly affect the detected discriminator output. These facts are important if one intends to apply the discrimination schemes to systems with wide-angle, mainly fan-beam, influence patterns. For such systems, return-pulse shape alterations (relative to the transmitter pulse shape) will occur because of the angular extension of the illuminated regions of target and aerosol.

The use of fan-beam influence patterns is the most direct approach to air-target fuzing applications. In the Navy and Air Force Sidewinder missiles, the optical fuze employs four 90-deg fan-beam systems to obtain full 360-deg coverage. A similar multisector approach is a basic design feature for a short-range, aerosol-resistant air-target optical fuze being designed at HDL. Because return-pulse shape-distortion effects not envisioned for pencil-beam systems will occur with fan beams, it is necessary to determine these effects and their impact on the aerosol-discrimination schemes that might be used, before intelligent design of aerosol-resistant fan-beam systems can be accomplished. Work along these lines is in progress.

A modeling capability for calculating target- and aerosol-return signals in fan-beam systems has been developed. This capability is now being used to determine the efficacy of the low-pass filter discrimination scheme for systems with various fan angles. The results of this work will appear in several future publications.

LITERATURE CITED

(1) H. H. Burroughs, Computation of Cloud Backscatter Power as a Function of Time for an Active Optical Radar (U), Naval Weapons Center, NWC TP 5090 (April 1971). (CONFIDENTIAL)

(2) R. E. Bird, Calculations of Multiple-Scattering Effects on Active Optical Sensors in Cloud Environments, Naval Weapons Center, NWC TP 5667 (August 1974).

(3) Z. G. Sztankay, Analysis of a Slant-Range Optical Proximity Sensor, Harry Diamond Laboratories, HDL-TR-1625 (July 1973).

(4) Wilbur B. Davenport, Jr., and William L. Root, An Introduction to the Theory of Random Signals and Noise, McGraw-Hill Book Co., Inc., New York (1958).

(5) E. Reisman and J. Pope, Final Report, Laser Polarization Scattering Studies, prepared by Philco-Ford Corp., under contract No. N00123-72-0244, for Naval Weapons Center (November 1972).

(6) J. Manz, A Ladar Cloud/Target Polarization Discrimination Technique, Air Force Systems Command, AFWL-TR-70-76 (October 1970).

(7) Z. G. Sztankay and D. W. McGuire, Backscatter in Clouds at 0.9 μm and its Effects on Optical Fuzing Systems, Proc. of Seventh DoD Conference on Laser Technology (November 1977).

(8) D. Deirmendjian, Electromagnetic Scattering on Spherical Polydispersions, American Elsevier Publishing Co. (1969).

(9) D. W. McGuire, H. M. Smalley, and Z. G. Sztankay, Measurements of Backscatter Effects in Clouds at 0.9 μm, Proc. of JTCG/MD/WPFF Tri-Service Optical Fuze Technology Symposium (October 1976).

(10) D. A. Giglio, B. J. Rod, and H. M. Smalley, Nephelometer Mapping of Backscatter and Attenuation Coefficients of Clouds, Harry Diamond Laboratories, HDL-TR-1660 (February 1974).

APPENDIX A.--SERIES REPRESENTATION OF OUTPUT OF DIFFERENTIATION CIRCUIT

This appendix derives a useful series expansion formula for the output of the differentiation circuit shown in figure 1 in the body of the report, and then applies the formula to a particular shape of the input voltage pulse to get a closed-form estimate of the departure of the output from the derivative of the input.

The series expansion formula is

$$R_T i_p(t) = \tau \frac{dv}{dt} - \tau^2 \frac{d^2v}{dt^2} + \tau^3 \frac{d^3v}{dt^3} - \tau^4 \frac{d^4v}{dt^4} + \cdots \quad , \qquad \text{(A-1)}$$

where it will be recalled that τ (which equals $R_T C$) is the overall circuit time constant, R_T (which equals $R_S + R$) is the total resistance, i_p is the nontransient part of the current i, and v(t) is the driving voltage signal. To derive equation (A-1) we use the result

$$i_p(t) = \frac{1}{R_T} \int_{-\infty}^{+\infty} \frac{A(\omega)}{\sqrt{1 + \dfrac{1}{\omega^2\tau^2}}} \sin\left[\omega t + \alpha(\omega) + \tan^{-1}(1/\omega\tau)\right] d\omega \qquad \text{(A-2)}$$

(eq (4) of the main text), which expresses i_p in terms of the amplitude and phase spectra, $A(\omega)$ and $\alpha(\omega)$, of v(t) (see eq (3)). Equation (A-2) is easily verified by substitution into the basic differential equation governing the circuit. We will assume that $A(\omega)$ vanishes outside some bounded interval $J = [\omega_l, \omega_u]$ and that $\omega^2\tau^2 < 1$ for all ω in this interval. Thus we are assuming that v(t) is band limited in a particular way.

To obtain the desired result, we first use the fact that

$$\sin\left[\omega t + \alpha(\omega) + \tan^{-1}(1/\omega\tau)\right] = \cos(\omega t + \alpha) \sin \tan^{-1}(1/\omega\tau) + \sin(\omega t + \alpha) \cos \tan^{-1}(1/\omega\tau), \qquad \text{(A-3)}$$

and that

$$\sin \tan^{-1}(1/\omega\tau) = 1/\left(1 + \omega^2\tau^2\right)^{1/2} \tag{A-4}$$

$$\cos \tan^{-1}(1/\omega\tau) = \omega\tau/\left(1 + \omega^2\tau^2\right)^{1/2} \,, \tag{A-5}$$

which show that equation (A-2) can be written as

$$\begin{aligned} R_T i_p(t) = & \int_{\omega_1}^{\omega_u} \frac{\omega\tau A(\omega)}{1 + \omega^2\tau^2} \cos\,[\omega t + \alpha(\omega)]\; d\omega \\ & + \int_{\omega_1}^{\omega_u} \frac{\omega^2\tau^2 A(\omega)}{1 + \omega^2\tau^2} \sin\,[\omega t + a(\omega)]\; d\omega \quad . \end{aligned} \tag{A-6}$$

Since $\omega^2\tau^2 < 1$ over the indicated integration range (by assumption), it is valid to introduce the expansion

$$\left(1 + \omega^2\tau^2\right)^{-1} = 1 - \omega^2\tau^2 + \omega^4\tau^4 - \omega^6\tau^6 + \ldots \tag{A-7}$$

in the above integrals and do the integrations term by term. Thus

$$\begin{aligned} R_T i_p(t) = & \sum_{n=0}^{\infty} (-1)^n \tau^{2n+1} \int_{\omega_1}^{\omega_u} \omega^{2n+1} A(\omega) \cos\,[\omega t + \alpha(\omega)]\; d\omega \; + \\ & + \sum_{n=1}^{\infty} (-1)^{n+1} \tau^{2n} \int_{\omega_1}^{\omega_u} \omega^{2n} A(\omega) \sin\,[\omega t + \alpha(\omega)]\; d\omega \quad . \end{aligned} \tag{A-8}$$

It is now easy to see that the desired result follows by noting that

$$\frac{d^{2n}v}{dt^{2n}} = (-1)^n \int_{\omega_1}^{\omega_u} \omega^{2n} A(\omega) \sin\,[\omega t + \alpha(\omega)]\; d\omega \quad , \tag{A-9}$$

and

$$\frac{d^{2n+1}v}{dt^{2n+1}} = (-1)^n \int_{\omega_1}^{\omega_u} \omega^{2n+1} A(\omega) \cos\,[\omega t + \alpha(\omega)]\, d\omega \quad . \qquad \text{(A-10)}$$

It should be pointed out that for $R = R_S = 50$ ohms and $C = 1$ pF we have $\tau = 10^{-10}$ s, so that if v(t) has the reasonable (for a 5-ns pulse) band limits $f_u = -f_1 \approx 200$ MHz ($\omega = 2\pi f$), the requirement that $\omega_u^2\tau^2 < 1$ is satisifed with a good margin.

We now argue the validity of equation (A-1) when v(t) is not band limited as was assumed. We will, however, need another assumption. Sufficient conditions for equation (A-1) to give a particular solution of the basic differential equation are (a) the series on the right of equation (A-1) converges, and (b) the time derivative of the function to which it converges is given by the term-by-term derivative of subject series. If these conditions hold for the v(t) in question, then direct substitution of equation (A-1) into equation (1) can be used to verify that the former is indeed a particular solution. Thus, equation (A-1) is valid if its right-hand side can be legitimately differentiated termwise.

The termwise differentiability of function series is ordinarily a delicate analytical question; however, in the case at hand it can be shown to be legitimate if the series on the right of equation (A-1) converges uniformly in a neighborhood of each fixed $t \varepsilon (-\infty, \infty)$. This will be our new assumption about v(t). The proof depends on the particular form of the series in question and on a standard result from advanced calculus.[1] We state the latter in a weakened form suitable for our purposes, for a series $\Sigma f_n(t)$ where each $f_n(t)$ is defined for $a < t < b$.

Proposition: Suppose that $\Sigma f_n(t)$ converges uniformly to a function f(t) on (a,b) and that $\Sigma f'_n(t)$ (where the prime denotes differentiation with respect to t) converges uniformly to a function g(t) on (a,b). Then $f'(t) = g(t)$ for each $t \varepsilon (a,b)$.

[1] *T. M. Apostol, Mathematical Analysis, Addison-Wesley Pub. Co., Inc. (1957), pp 401-403.*

APPENDIX A

We apply the foregoing proposition to our problem by putting $f_n(t) = (-1)^{n+1}\ \tau^n(d^n v/dt^n)$ and assume that $\Sigma f_n(t)$ converges uniformly in a neighborhood of each fixed $t_o \varepsilon(-\infty,\infty)$. One readily sees that the derived series

$$\Sigma f_n'(t) = \frac{dv}{dt} - \frac{1}{\tau} f(t) \quad , \tag{A-11}$$

so that it has the same uniform convergence property as $\Sigma f_n(t) = f(t)$ on the neighborhood in question. It therefore follows from the proposition that

$$\Sigma f_n'(t) = f'(t) \tag{A-12}$$

for all t in the neighborhood.

Because of the foregoing, equation (A-1) can be applied to the v(t) given by equation (6) in the body of the report even though this v(t) is not band limited. This can be seen as follows.

It is readily verified that

$$\frac{d^{2n}v}{dt^{2n}} = (-1)^{n+1}\left(\frac{\pi}{T}\right)^{2n-2} \frac{d^2v}{dt^2} \quad , \tag{A-13}$$

for n = 1, 2, 3 ..., and that

$$\frac{d^{2n+1}v}{dt^{2n+1}} = (-1)^n\left(\frac{\pi}{T}\right)^{2n} \frac{dv}{dt} \quad , \tag{A-14}$$

for n = 0, 1, 2, ... Denote the right-hand side of equation (A-1) by D(t). Upon substitution of the above results into the right-hand side of equation (A-1), one gets

$$D(t) = \left(\tau \frac{dv}{dt} - \tau^2 \frac{d^2v}{dt^2}\right) \sum_{n=0}^{\infty} (-1)^n q^{2n} \quad , \tag{A-15}$$

where

$$q = \frac{\pi\tau}{T} \quad .$$

Therefore,

$$D(t) = \frac{1}{1 + q^2}\left(\tau \frac{dv}{dt} - \tau^2 \frac{d^2v}{dt^2}\right) \quad , \tag{A-16}$$

provided $\pi\tau/T < 1$, because the series in equation (A-15) is a geometric series. Since the proviso certainly holds for $T = 5$ ns and $\tau = 10^{-10}$ s, equation (A-16) gives the uniform limit of the right-hand side of equation (A-1). Thus equation (A-1) applies to the v(t) in question, and we have

$$R_T i_p(t) = \tau \frac{dv}{dt}\left(\frac{1}{1 + q^2}\right) - \tau^2 \frac{d^2v}{dt^2}\left(\frac{1}{1 + q^2}\right) . \tag{A-17}$$

Equation (A-17), which is equation (7) of the main text, gives an estimate of the departure of the differentiator output from the derivative of the input.

APPENDIX B.--FORTRAN LISTING OF PROGRAM FOR CALCULATING AEROSOL-RETURN SIGNALS

This appendix contains a listing of the computer program discussed in section 2.2 of the main body of the report. The main part of the program handles the computation of the integral in equation (10), sets up plotting arrays, and provides various other computational and outputting options. The range-response functions are provided by the two subroutines named RANGER and RANGES. The function C(x) of equation (9) is provided by the function subprogram CLOUD; the time variation of the transmitter pulse is provided by the function subprogram P(X,W).

The subroutine RANGER gives the range-response function for systems where the transmitter optics focuses the optical source at a definite range (R1 in the program) from the system, and similarly the receiver optics focuses the active photodetector surface at the same range. The analysis which leads to the subroutine is unpublished. It takes into account finite separation distances between transmitter and receiver optics, and assumes rectangular-shaped lenses for simplicity. A published analysis for circular lenses where transmitter and receiver are assumed coaxial is given by Humphrey.[1]

The subroutine RANGES gives the range response obtained with uniform overlapping pencil beams, as discussed in the body of this report. The approximate formulation of such range laws is straightforward.

The program variable name for the aerosol extinction coefficient σ is ALPHA. Both the symbols σ and α are routinely used to designate the extinction coefficient. There is now an attempt afoot to standardize the use of σ for this purpose.

---

[1] *R. G. Humphrey, Properties of an Active Optical System, Harry Diamond Laboratories, HDL-TR-1281 (April 1965).*

APPENDIX B

```
      DIMENSION V(1002),DV(1001),CR(1002),RR(1002),DRR(1001),BASE(4)
      DIMENSION NOTE1(14),NOTE2(14),NOTE3(10),NOTE4(20),NOTE5(14)
      REAL MU
      DATA C,IYTXT,BASE/.299776,'Y',-1.,3*0./,DRR(2),DV(2)/2*0./
C
C   DEFINE ASCII-DECIMAL-EQUIVALENT TEXT FOR PLOTTING
C
C              R  E  L  A  T  I  V  E     R  A  N  G  E
      DATA NOTE1/82,69,76,65,84,73,86,69,32,82,65,78,71,69/
C
C              R  T  N     P  W  R  (  .  1  T  G  T  )
      DATA NOTE2/82,84,78,32,80,87,82,40,46,49,84,71,84,41/
C
C              D  E  R  I  V  A  T  I  V  E
      DATA NOTE3/68,69,82,73,86,65,84,73,86,69/
C
C              C  L  O  U  D     S  I  G  *  R  A  N  G  E     R  E
      DATA NOTE4/67,76,79,85,68,32,83,73,71,42,82,65,78,71,69,32,82,69,
C
C        S  P
     *   83,80/
C
C              R  A  N  G  E     R  E  S  P  O  N  S  E
      DATA NOTE5/82,65,78,71,69,32,82,69,83,80,79,78,83,69/
C
C
C   PROGRAM VARIABLES
C
C     V          AEROSOL RETURN POWER SAMPLED AT PERIOD T
C                (REL TO STD TARGET OF .1 AT R1)
C     DV         DERIVATIVE OF CONVOLVED RESPONSE
C     CR         PRODUCT OF THE CLOUD AND RANGE RESPONSES
C     RR         RANGE RESPONSE
C     DRR        DERIVATIVE OF RANGE RESPONSE
C     BASE       TIME BASE ARRAY FOR PLOTTING
C     C          SPEED OF LIGHT IN METERS/NANOSECOND
C     W          FULL BASE WIDTH OF THE SOURCE PULSE
C     XO,X1      BOUNDARY DISTANCES FOR THE CLOUD MODEL IN METERS
C     ALPHA,MU   ABSORPTION AND BACKSCATTER COEFFICIENTS FOR CLOUD
C     T          SAMPLING PERIOD IN NANOSECONDS
C     NPTS       NUMBER OF SAMPLES TO BE CALCULATED
C
      CALL TPUTAS('BAUD RATE',9,IER)
      READ *,ITERM
      CALL INITT(ITERM/10)
      CALL ANMODE
      WRITE (6,6005)
 6005 FORMAT (' IS THE LARGE SCREEN BEING USED?')
      CALL TPUTAS('ENTER Y OR N: ',14,IER)
      READ (5,5000) ITERM
      IF (ITERM.NE.IYTXT) GO TO 5
      CALL TERM(3,4096)
      CALL CHRSIZ(1)
```

```
5     CALL NEWPAG
      CALL ANMODE
C
C   READ IN PROBLEM PARAMETERS
C
      WRITE(6,7000)
7000  FORMAT(' IS SIMPLE WANTED?')
      CALL TPUTAS('ENTER Y OR N: ',14,IER)
      READ(5,5000) IANS
      IF(IANS.NE.IYTXT) GO TO 10
11    CALL RANGES(R1,D,RX,RY,Q)
      GO TO 12
10    CALL RANGER(R1,D,RX,RY,Q)
12    WRITE(6,6000)
6000  FORMAT (' DO YOU WISH TO CALCULATE CLOUD RESPONSE?')
      CALL TPUTAS('ENTER Y OR N: ',14,IER)
      READ (5,5000) ICLD
5000  FORMAT (A1)
      IF (ICLD.NE.IYTXT) GO TO 20
      CALL TPUTAS('PULSE BASE WIDTH (NANOSECONDS)',30,IER,1)
      READ *,W
      CALL TPUTAS('CLOUD BOUNDARY RANGES - X0 AND X1 (METERS)',42,
     *   IER,1)
      READ *,X0,X1
      CALL TPUTAS('ALPHA AND MU',12,IER,1)
      READ *,ALPHA,MU
20    CALL TPUTAS('SAMPLING PERIOD (NANOSECONDS)',29,IER,1)
      READ *,T
      CALL TPUTAS('NUMBER OF SAMPLES (1001 MAX)',28,IER,1)
      READ *,NPTS
C
C   SET UP ARRAYS FOR PLOTTING
C
      BASE(2)=NPTS
      RR(1)=NPTS
      DRR(1)=NPTS-1
      CR(1)=NPTS
      V(1)=NPTS
      DV(1)=NPTS-1
      BASE(4)=C*T/(2.*R1)
      NPT=NPTS+1
C
C   CALCULATE RR AND DRR ARRAYS.  RNORM IS A NORMALIZING FACTOR SO
C   THAT THE RESPONSE AT R1 FOR ANY RX,RY IS 1.
C
      RNORM=RX*RY*D**6/(2.*R1**4)
      DO 30 I=2,NPT
      IF(IANS.NE.IYTXT) GO TO 22
      CALL RANGES(C*T*FLOAT(I-2)/2.,RR(I))
      GO TO 23
22    CALL RANGE(C*T*FLOAT(I-2)/2.,RR(I))
23    RR(I)=RR(I)/RNORM
      IF (I.GT.3) DRR(I-1)=(RR(I)-RR(I-2))/(2.*T)
30    CONTINUE
C
C   IF RESPONSE IS DESIRED, CALCULATE CR, V AND DV ARRAYS
C
      IF (ICLD.NE.IYTXT) GO TO 60
      DO 35 I=2,NPT
      CR(I)=CLOUD(C*T*FLOAT(I-2)/2.,X0,X1,ALPHA,MU)*RR(I)
```

```
35    CONTINUE
      DO 50 I=2,NPT
      N=I-3
      IO=MAX1(0.,2.*XO/(C*T),FLOAT(N)-W/T)+1
      V(I)=0.
C
C   LOOP THROUGH CONVOLUTION SUM
C
      DO 40 J=IO,N
      V(I)=V(I)+P(FLOAT(N-J+1)*T,W)*CR(J+2)
40    CONTINUE
      V(I)=V(I)*T*(3.14159267*C/(2.*.1))
C
C    V IS THE AEROSOL RETURN POWER AS A FUNCTION
C    OF TIME, RELATIVE TO THE PEAK RECEIVED POWER
C    FROM A 0.1 REFLECTIVITY DIFFUSE TARGET AT THE
C    IMAGE PLANE DISTANCE R1
      IF (I.GT.3) DV(I-1)=(V(I)-V(I-2))/(2.*T)
50    CONTINUE
C
C   PLOT RESULTS
C
60    CALL NEWPAG
      CALL ANMODE
      CALL MENU(I,ICLD)
      IF (I.EQ.0) GO TO 130
      CALL NEWPAG
      CALL BINITT
      CALL SLIMY(IFIX(COMGET(IBASEY(13))),IFIX(.9*(COMGET(IBASEY(14))-
     *   COMGET(IBASEY(13)))+COMGET(IBASEY(13))))
      CALL TITLE(R1,D,RX,RY,Q,XO,X1,ALPHA,MU,W,T,NPTS,ICLD)
      CALL NOTATE((IFIX(COMGET(IBASEX(13))+COMGET(IBASEX(14)))-
     *   LINWDT(14))/2,40,14,NOTE1)
      GO TO (70,80,90,100,110),I
C
C   PLOT RETURN SIGNAL
C
70    CALL MOVABS(LINWDT(2),
     *   (IFIX(COMGET(IBASEY(13))+COMGET(IBASEY(14)))+LINHGT(14))/2)
      CALL VLABEL(14,NOTE2)
      CALL CHECK(BASE,V)
      CALL DSPLAY(BASE,V)
      GO TO 120
C
C   PLOT DERIVATIVE OF RETURN SIGNAL
C
80    CALL MOVABS(LINWDT(2),
     *   (IFIX(COMGET(IBASEY(13))+COMGET(IBASEY(14)))+LINHGT(25))/2)
      CALL VLABEL(14,NOTE2)
      CALL MOVABS(LINWDT(2),
     *   (IFIX(COMGET(IBASEY(13))+COMGET(IBASEY(14)))-LINHGT(5))/2)
      CALL VLABEL(10,NOTE3)
      CALL CHECK(BASE,DV)
      CALL DSPLAY(BASE,DV)
      GO TO 120
C
C   PLOT CLOUD RESPONSE
C
90    CALL MOVABS(LINWDT(2),
     *   (IFIX(COMGET(IBASEY(13))+COMGET(IBASEY(14)))+LINHGT(20))/2)
```

```
      CALL VLABEL(20,NOTE4)
      CALL CHECK(BASE,CR)
      CALL DSPLAY(BASE,CR)
      GO TO 120
C
C   PLOT RANGE RESPONSE
C
100   CALL MOVABS(LINWDT(2),
     *    (IFIX(COMGET(IBASEY(13))+COMGET(IBASEY(14)))+LINHGT(14))/2)
      CALL VLABEL(14,NOTE5)
      CALL CHECK(BASE,RR)
      CALL OSPLAY(BASE,RR)
      GO TO 120
C
C   PLOT DERIVATIVE OF RANGE RESPONSE
C
110   CALL MOVABS(LINWDT(2),
     *    (IFIX(COMGET(IBASEY(13))+COMGET(IBASEY(14)))+LINHGT(25))/2)
      CALL VLABEL(14,NOTE5)
      CALL MOVABS(LINWDT(2),
     *    (IFIX(COMGET(IBASEY(13))+COMGET(IBASEY(14)))-LINHGT(5))/2)
      CALL VLABEL(10,NOTE3)
      CALL CHECK(BASE,ORR)
      CALL OSPLAY(BASE,ORR)
C
C   PLOT DONE - PAUSE
C
120   CALL BELL
      CALL TINPUT(I)
      GO TO 60
C
C   PROBLEM FINISHED - ASK FOR ANOTHER
C
130   WRITE (6,6010)
6010  FORMAT (' DO YOU WANT ANOTHER PROBLEM?')
      CALL TPUTAS('ENTER Y OR N:',14,IER)
      REAO (5,5000) I
      IF (I.NE.IYTXT) GO TO 139
      IF((I.EQ.IYTXT).AND.(IANS.NE.IYTXT)) GO TO 10
      GO TO 11
139   CALL NEWPAG
      IF (ITERM.NE.IYTXT) GO TO 140
      CALL CHRSIZ(4)
      CALL FINITT(0,3080)
140   CALL FINITT(0,767)
      STOP
      ENO
```

```
      SUBROUTINE TITLE(R1,D,RX,RY,Q,X0,X1,ALPHA,MU,W,T,NPTS,ICLD)
      REAL MU
      DIMENSION ITXT1(53),ITXT2(46),ITXT3(47)
      DATA IYTXT/'Y'/
C
C   DEFINE ASCII-DECIMAL-EQUIVALENT TEXT FOR TITLES
C
C                R (SUB)1    =       D  =       Q  =       R (SUB)X
      DATA ITXT1/82,-2,49,-1,61,7*32,68,61,7*32,81,61,7*32,82,-2,120,-1,
C
C         =      R (SUB)Y     =
     *   61,7*32,82,-2,121,-1,61,6*32/
C
C                X (SUB)0    =       X (SUB)1    =       A  L  P  H  A
      DATA ITXT2/88,-2,48,-1,61,7*32,88,-2,49,-1,61,7*32,65,76,80,72,65,
C
C         =      M  U  =
     *   61,7*32,77,85,61,6*32/
C
C                P  U  L  S  E    W  I  D  T  H  =       S  A  M
      DATA ITXT3/80,85,76,83,69,32,87,73,68,84,72,61,7*32,83,65,77,
C
C        P  L  I  N  G  =       P  O  I  N  T  S
     *   80,76,73,78,71,61,13*32,80,79,73,78,84,83/
C
C   ENCODE TITLE INFORMATION
C
      CALL FFORM(R1,6,3,ITXT1(6),32)
      CALL FFORM(D,6,4,ITXT1(15),32)
      CALL FFORM(Q,6,3,ITXT1(24),32)
      CALL FFORM(RX,6,3,ITXT1(36),32)
      CALL FFORM(RY,6,3,ITXT1(48),32)
      IF (ICLD.NE.IYTXT) GO TO 10
      CALL FFORM(X0,6,3,ITXT2(6),32)
      CALL FFORM(X1,6,3,ITXT2(18),32)
      CALL FFORM(ALPHA,6,3,ITXT2(31),32)
      CALL FFORM(MU,6,4,ITXT2(41),32)
      CALL FFORM(W,6,2,ITXT3(13),32)
 10   CALL FFORM(T,6,4,ITXT3(29),32)
      CALL IFORM(FLOAT(NPTS),4,ITXT3(37),32)
C
C   DISPLAY TITLES
C
      CALL SEETRM(IA,IB,IC,ID)
      ITOP=780
      IF (ID.EQ.4095) ITOP=3120
      CALL NOTATE(IFIX(COMGET(IBASEX(13))),ITOP-LINHGT(1),53,ITXT1)
      IF (ICLD.NE.IYTXT) GO TO 20
      CALL NOTATE(IFIX(COMGET(IBASEX(13))),
     *   ITOP-LINHGT(2)-LINHGT(1)/2,46,ITXT2)
      CALL NOTATE(IFIX(COMGET(IBASEX(13))),
     *   ITOP-LINHGT(4),47,ITXT3)
      RETURN
```

```
20    CALL NOTATE(IFIX(COMGET(IBASEX(13))),
     *   ITOP-LINHGT(2)-LINHGT(1)/2,28,ITXT3(20))
      RETURN
      END
```

```
      SUBROUTINE MENU(I,ICLD)
      DATA IYTXT/'Y'/,IPTR/0/
      DIMENSION IARRAY(5)
      IF (IPTR.NE.0) GO TO 40
C
C   DISPLAY APPROPRIATE MENU
C
10    IF (ICLD.NE.IYTXT) GO TO 20
      WRITE (6,6000)
6000  FORMAT (' THE FOLLOWING OPTIONS ARE AVAILABLE:'//
     *   5X,'1 - AEROSOL RETURN'/
     *   5X,'2 - AEROSOL RETURN DERIVATIVE'/
     *   5X,'3 - CLOUD*RANGE RESPONSE'/
     *   5X,'4 - RANGE RESPONSE'/
     *   5X,'5 - RANGE RESPONSE DERIVATIVE'/)
      GO TO 30
20    WRITE (6,6010)
6010  FORMAT (' THE FOLLOWING OPTIONS ARE AVAILABLE:'//
     *   5X,'1 - RANGE RESPONSE'/
     *   5X,'2 - RANGE RESPONSE DERIVATIVE'/)
30    CALL TPUTAS('ENTER LIST OF OPTIONS: ',23,IER)
      READ (5,5000,ERR=30) IARRAY
5000  FORMAT (5(I1,1X))
C
C   GET NEXT OPTION FROM LIST
C
40    IPTR=IPTR+1
      IF (IPTR.GT.5) GO TO 50
      I=IARRAY(IPTR)
      IF (I.EQ.0.OR.I.GT.5) GO TO 50
      IF (I.GT.2.AND.ICLD.NE.IYTXT) GO TO 50
      IF (ICLD.NE.IYTXT) I=I+3
      RETURN
C
C   NO MORE LEGAL OPTIONS - END PROBLEM
C
50    IPTR=0
      I=0
      RETURN
      END
```

APPENDIX B

```
      FUNCTION P(X,W)
      P=0.
      IF (X.GT.0..AND.X.LT.W) P=SIN(3.1415926536*X/W)**2
      RETURN
      END
```

```
      FUNCTION CLOUD(X,X0,X1,ALPHA,MU)
      REAL MU
      CLOUD=0.
      IF (X.GE.X0.AND.X.LT.X1) CLOUD=MU*(X-X0)*EXP(-ALPHA*(X-X0)**2/
     *   (X1-X0))/(X1-X0)
      IF (X.GE.X1) CLOUD=MU*EXP(-ALPHA*(2.*X-X0-X1))
      RETURN
      END
```

```
      SUBROUTINE REXP(X,R,D,R1,RX,RY)
      COMMON/LLINE/ SL,YINT
      R=0.
      IF (X.LT.0..OR.X.GT.R1) RETURN
      R=SL*X+YINT
C
C     R MULTIPLIED BY FACTOR TO NULL RNORM IN MAIN
C
      R=R*RX*RY*(D**6)/(2.*R1**4)
      RETURN
      END
```

```
      SUBROUTINE RANGER(R1,D,RX,RY,Q)
      DIMENSION ENDX(8),ENDY(3)
      REAL INFNTY/1.E50/
      COMMON/LLINE/ SL,YINT
      DATA IYTXT/'Y'/
      X1(X)=D*(2.+Q-X*(2.+Q+RX)/R1)/2.
      X2(X)=D*(2.+Q-X*(2.+Q-RX)/R1)/2.
      X3(X)=D*(Q-X*(Q-RX)/R1)/2.
      X4(X)=D*(Q-X*(Q+RX)/R1)/2.
      Y2(X)=D*(1.-X*(1.-RY)/R1)/2.
      Y3(X)=D*(-1.+X*(1.+RY)/R1)/2.
C
C   INPUT PARAMETERS FOR FSOS RANGE MODEL
C
      WRITE (6,6000)
6000  FORMAT (' INPUT RANGE RESPONSE PARAMETERS:')
      CALL TPUTAS('R1 (METERS)',11,IER,1)
      READ *,R1
      CALL TPUTAS('D (METERS)',10,IER,1)
      READ *,D
      CALL TPUTAS('Q',1,IER,1)
      READ *,Q
      CALL TPUTAS('RX',2,IER,1)
      READ *,RX
      CALL TPUTAS('RY',2,IER,1)
      READ *,RY
      R0=0.
      SL=0.
      YINT=0.
      WRITE(6,7000)
7000  FORMAT(' DO YOU WANT TO MODIFY THE IN RANGE HOLE?')
      CALL TPUTAS('ENTER Y OR N: ',14,IER)
      READ(5,7001) IANS
7001  FORMAT(A1)
      IF(IANS.NE.IYTXT) GO TO 5
      CALL TPUTAS('RANGE TO BEGIN USING THEORETICAL RANGE RESPONSE',47,
     *   IER,1)
      READ *,R0
      CALL TPUTAS('ENTER SLOPE AND Y-INT',21,IER,1)
      READ *, SL,YINT
C
C   CALCULATE X TERM INTERVAL END POINTS
C
5     S=R1*Q/(Q+RX)
      ENDX(1)=R1/(1.+RX)
      IF (Q.GT.1.) ENDX(1)=S
      ENDX(2)=R1*(1.+Q)/(1.+Q+RX)
      ENDX(3)=R1*(2.+Q)/(2.+Q+RX)
      ENDX(4)=R1
      ENDX(5)=INFNTY
      IF (RX.LT.Q+2.) ENDX(5)=R1*(2.+Q)/(2.+Q-RX)
      ENDX(6)=INFNTY
      IF (RX.LT.Q+1.) ENDX(6)=R1*(1.+Q)/(1.+Q-RX)
```

```
      ENDX(7)=INFNTY
      IF (Q.LT.1..AND.RX.LT.1.) ENDX(7)=R1/(1.-RX)
      ENDX(8)=INFNTY
      IF (RX.LT.Q) ENDX(8)=R1*Q/(Q-RX)
      IF (Q.GT.1.) ENDX(7)=ENDX(8)
C
C   CALCULATE Y TERM INTERVAL END POINTS
C
      ENDY(1)=R1/(1.+RY)
      ENDY(2)=R1
      ENDY(3)=INFNTY
      IF (RY.LT.1.) ENDY(3)=R1/(1.-RY)
      RETURN
      ENTRY RANGE(X,R)
C
C   CALCULATE RETURN
C
      R=0.
      IF (X.GE.R0) GO TO 10
C
C   GET RANGE RESPONSE FROM USER SUPPLIED ROUTINE 'REXP'
C
      CALL REXP(X,R,D,R1,RX,RY)
      RETURN
C
C   USE THEORETICAL RANGE RESPONSE FORMULA
C
10    IF (X.LE.S.OR.X.GE.ENDX(8)) RETURN
C
C   CALCULATE X TERM OF THEORETICAL RESPONSE
C
      IF (X.GT.ENDX(1)) GO TO 20
      XTERM=((RX*D/(R1-X))**2)*(-4.*X4(X)**3/(3.*(X3(X)-X4(X))**2))
      GO TO 90
20    IF (X.GT.ENDX(2)) GO TO 30
      XTERM=((D/X)**2)*(-4.*X4(X)**3/(3.*(X1(X)-X4(X))**2))
      GO TO 90
30    IF (X.GT.ENDX(3)) GO TO 40
      XTERM=((D/X)**2)*((-4.*X4(X)**3+(X1(X)+X4(X))**3)/
     *   (3.*(X1(X)-X4(X))**2))
      GO TO 90
40    IF (X.GT.ENDX(4)) GO TO 50
      XTERM=((D/X)**2)*(-X1(X)-X4(X))
      GO TO 90
50    IF (X.GT.ENDX(5)) GO TO 60
      XTERM=((D/X)**2)*(X2(X)+X3(X))
      GO TO 90
60    IF (X.GT.ENDX(6)) GO TO 70
      XTERM=((D/X)**2)*((4.*X3(X)**3-(X2(X)+X3(X))**3)/
     *   (3.*(X2(X)-X3(X))**2))
      GO TO 90
70    IF (X.GT.ENDX(7)) GO TO 80
      XTERM=((D/X)**2)*(4.*X3(X)**3/(3.*(X3(X)-X2(X))**2))
      GO TO 90
80    XTERM=((RX*D/(R1-X))**2)*(4.*X3(X)**3/(3.*(X3(X)-X4(X))**2))
C
C   COMPUTE Y TERM OF THEORETICAL RESPONSE
C
90    IF (X.GT.ENDY(1)) GO TO 100
      YTERM=((RY*D/(R1-X))**2)*((Y2(X)-2.*Y3(X))/3.)
```

```
      GO TO 130
100   IF (X.GT.ENDY(2)) GO TO 110
      YTERM=((D/X)**2)*((Y2(X)+2.*Y3(X))/3.)
      GO TO 130
110   IF (X.GT.ENDY(3)) GO TO 120
      YTERM=((D/X)**2)*((Y3(X)+2.*Y2(X))/3.)
      GO TO 130
120   YTERM=((RY*D/(R1-X))**2)*((Y3(X)-2.*Y2(X))/3.)
C
C   COMPUTE THEORETICAL RESPONSE
C
130   R=XTERM*YTERM
      RETURN
      END
```

```
      SUBROUTINE RANGES(R0,RF,RX,RY,Q)
C
C   INPUT PARAMETERS FOR SIMPLE RANGE MODEL
C
      WRITE (6,6000)
6000  FORMAT (' INPUT RANGE RESPONSE PARAMETERS - SIMPLE MODEL')
      CALL TPUTAS('R0 (METERS): ',13,IER,1)
      READ *,R0
      CALL TPUTAS('RF (METERS): ',13,IER,1)
      READ *,RF
      C=1.-R0/RF
C
C   RX,RY SET TO 1. TO NULL RNORM IN MAIN
C
      RX=1.
      RY=1.
      Q=0.
      RETURN
      ENTRY RANGES(X,R)
C
C   CALCULATE RETURN
C
      R=0.
      IF (X.GE.R0.AND.X.LE.RF) R=(1.-R0/X)/(X*X*C)
      IF (X.GT.RF) R=1./(X*X)
C
C   R MULTIPLIED BY FACTOR TO NULL RNORM IN MAIN
C
      R=R*(RF**6/(2.*R0**4))
      RETURN
      END
```

DISTRIBUTION

ADMINISTRATOR
DEFENSE TECHNICAL INFORMATION CENTER
ATTN DTIC-DDA (12 COPIES)
CAMERON STATION, BUILDING 5
ALEXANDRIA, VA 22314

COMMANDER
US ARMY RSCH & STD GP (EUR)
BOX 65
ATTN CHIEF, PHYSICS & MATH BRANCH
FPO NEW YORK 09510

COMMANDER
US ARMY ARMAMENT MATERIEL
READINESS COMMAND
ATTN DRSAR-LEP-L, TECHNICAL LIBRARY
ATTN DRSAR-ASF, FUZE & MUNITIONS
SUPPORT DIVISION
ROCK ISLAND, IL 61299

COMMANDER
US ARMY MISSILE & MUNITIONS
CENTER & SCHOOL
ATTN ATSK-CTD-F
REDSTONE ARSENAL, AL 35809

DIRECTOR
US ARMY MATERIEL SYSTEMS ANALYSIS ACTIVITY
ATTN DRXSY-MP
ABERDEEN PROVING GROUND, MD 21005

DIRECTOR
US ARMY BALLISTIC RESEARCH LABORATORY
ATTN DRDAR-TSB-S (STINFO)
ABERDEEN PROVING GROUND, MD 21005

TELEDYNE BROWN ENGINEERING
CUMMINGS RESEARCH PARK
ATTN DR. MELVIN L. PRICE, MS-44
HUNTSVILLE, AL 35807

ENGINEERING SOCIETIES LIBRARY
345 EAST 47TH STREET
ATTN ACQUISITIONS DEPARTMENT
NEW YORK, NY 10017

HQ USAF/SAMI
WASHINGTON, DC 20330

US ARMY ELECTRONICS TECHNOLOGY
AND DEVICES LABORATORY
ATTN DELET-DD
FORT MONMOUTH, NJ 07703

COMMANDER
US ARMY ARMAMENT RESEARCH
& DEVELOPMENT COMMAND
ATTN DRDAR-FU, ARMY FUZE MANAGEMENT
PROJECT OFFICER, LTC GRADY COOK
DOVER, NJ 07801

US ARMY ELECTRONICS RESEARCH
& DEVELOPMENT COMMAND
ATTN TECHNICAL DIRECTOR, DRDEL-CT

HARRY DIAMOND LABORATORIES
ATTN CO/TD/TSO/DIVISION DIRECTORS
ATTN RECORD COPY, 81200
ATTN HDL LIBRARY, 81100 (3 COPIES)
ATTN HDL LIBRARY, 81100 (WOODBRIDGE)
ATTN TECHNICAL REPORTS BRANCH, 81300
ATTN CHAIRMAN, EDITORIAL COMMITTEE
ATTN CHIEF, 13000
ATTN CHIEF, 11000
ATTN CHIEF, 13300
ATTN CHIEF, 11400
ATTN COX, L, 00211
ATTN HUMPHREY, R., 13300
ATTN GRIFFIN, J. R., 13300
ATTN HATTERY, W. V., 13300
ATTN VANDERWALL, J., 12300
ATTN SANN, K. H., 15000
ATTN PEPERONE, S. J., 42600
ATTN DOBRIANSKY, B., 13500 (2 COPIES)
ATTN LANHAM, C., 00210
ATTN GIGLIO, D., 15300
ATTN GEIPE, T., 22100
ATTN TUTTLE, J., 21400
ATTN MCGUIRE, D., 13300 (10 COPIES)
ATTN HOPP, T., 00251 (10 COPIES)
ATTN CONNER, M., 15200 (10 COPIES)